ANTIOXIDANTS & REDOX SIGNALING
Volume 34, Number 7, 2021

DOI: 10.1089/ars.2019.7929

Discoveries

FORUM ORIGINAL RESEARCH COMMUNICATION

The Determining Role of Mitochondrial Reactive Oxygen Species Generation and Monoamine Oxidase Activity in Doxorubicin-Induced Cardiotoxicity

Salvatore Antonucci,[1] Moises Di Sante,[1] Federica Tonolo,[1] Laura Pontarollo,[1] Valeria Scalcon,[1] Petra Alanova,[1,2] Roberta Menabò,[3] Andrea Carpi,[1] Alberto Bindoli,[3] Maria Pia Rigobello,[1] Marco Giorgio,[1,4] Nina Kaludercic,[3] and Fabio Di Lisa[1,3]

Abstract

Aims: Doxorubicin cardiomyopathy is a lethal pathology characterized by oxidative stress, mitochondrial dysfunction, and contractile impairment, leading to cell death. Although extensive research has been done to understand the pathophysiology of doxorubicin cardiomyopathy, no effective treatments are available. We investigated whether monoamine oxidases (MAOs) could be involved in doxorubicin-derived oxidative stress, and in the consequent mitochondrial, cardiomyocyte, and cardiac dysfunction.
Results: We used neonatal rat ventricular myocytes (NRVMs) and adult mouse ventricular myocytes (AMVMs). Doxorubicin alone (*i.e.*, 0.5 μM doxorubicin) or in combination with H_2O_2 induced an increase in mitochondrial formation of reactive oxygen species (ROS), which was prevented by the pharmacological inhibition of MAOs in both NRVMs and AMVMs. The pharmacological approach was supported by the genetic ablation of MAO-A in NRVMs. In addition, doxorubicin-derived ROS caused lipid peroxidation and alterations in mitochondrial function (*i.e.*, mitochondrial membrane potential, permeability transition, redox potential), mitochondrial morphology (*i.e.*, mitochondrial distribution and perimeter), sarcomere organization, intracellular $[Ca^{2+}]$ homeostasis, and eventually cell death. All these dysfunctions were abolished by MAO inhibition. Of note, *in vivo* MAO inhibition prevented chamber dilation and cardiac dysfunction in doxorubicin-treated mice.
Innovation and Conclusion: This study demonstrates that the severe oxidative stress induced by doxorubicin requires the involvement of MAOs, which modulate mitochondrial ROS generation. MAO inhibition provides evidence that mitochondrial ROS formation is causally linked to all disorders caused by doxorubicin *in vitro* and *in vivo*. Based upon these results, MAO inhibition represents a novel therapeutic approach for doxorubicin cardiomyopathy. *Antioxid. Redox Signal.* 34, 531–550.

Keywords: doxorubicin, cardiomyopathy, mitochondria, monoamine oxidase, reactive oxygen species (ROS)

Introduction

Doxorubicin (Adriamycin®) is a very efficient antineoplastic drug used in cancer treatment that belongs to the anthracycline family (44). Unfortunately, its therapeutic value is very much limited by a remarkable cardiotoxicity (21). The doxorubicin-derived cardiac dysfunction is dose dependent, and the resulting doxorubicin cardiotoxicity (DC) may arise even at low doses in an individual-dependent manner (33). Many mechanisms (21) have been suggested to explain doxorubicin anticancer properties, such as DNA intercalation (65), sarcopenia (40), adverse signaling (38),

[1]Department of Biomedical Sciences, University of Padova, Padova, Italy.
[2]Institute for Physiology, Czech Academy of Sciences, Prague, Czech Republic.
[3]Neuroscience Institute, National Research Council of Italy (CNR), Padova, Italy.
[4]European Institute of Oncology (IEO), Milan, Italy.

Innovation

Monoamine oxidase (MAO)-dependent reactive oxygen species (ROS) formation contributes to cardiomyocyte dysfunction by exacerbating doxorubicin-derived mitochondrial ROS. MAO inhibition demonstrates that mitochondrial ROS formation is upstream of doxorubicin-induced injury in cardiomyocytes and doxorubicin-treated hearts. This study suggests that MAOs may represent a promising target for novel therapeutic approaches for doxorubicin cardiotoxicity, which should be validated by clinical testing as well as by additional experimental studies.

impairment of intracellular [Ca^{2+}] homeostasis (32), and, above all, oxidative stress (65).

The two main metabolic pathways leading to anthracyclines-dependent formation of reactive oxygen species (ROS) are one-electron reduction, which generates superoxide (44), and two-electron reduction, which generates a secondary alcohol, DOXol (54). These two mechanisms are of great importance for the anticancer properties of doxorubicin, since the one-electron reduction occurs especially at the mitochondrial level, while the two-electron reduction is achieved mainly in the cytoplasm (54). However, all these mechanisms that are essential for cancer therapy become harmful when they are observed also in the myocardium, in which they were mostly reported as independent events by different laboratories, with hardly any attempt to achieve a unifying mechanism of DC (21).

In this respect, the major focus has been given to doxorubicin-induced oxidative stress (21, 62). Although doxorubicin induces ROS formation by different pathways, such as interacting with free iron (44), interacting with NAD(P)H oxidases (15), or binding to the endothelial nitric oxide synthase (44), this anthracycline is retained within the mitochondria as a result of its nearly irreversible binding to cardiolipin (69), making mitochondria both the source (20, 47) and the target of ROS (20, 73).

Doxorubicin-dependent formation of ROS within the mitochondria is related to its redox cycling activity at Complex I (6, 25) and to the consequent dysfunction of the electron transport chain (ETC) (25). Notably, we have recently demonstrated that another redox cycler at Complex I (MitoParaquat) causes a primary increase in mitochondrial ROS formation that is upstream of both mitochondrial and cellular abnormalities (2). The relevance of oxidative stress supports the use of the iron chelator and topoisomerase II inhibitor dexrazoxane, which is the only drug approved by the U.S. Food and Drug Administration against DC. Anthracycline–iron complexes are believed to promote myocyte-damaging free radicals, and thus dexrazoxane reduces cardiac toxicity in subjects treated with anthracyclines. However, far from enhancing the antitumor efficacy of doxorubicin, the therapeutic value of dexrazoxane is limited by the risk of secondary malignancies (41, 64).

Although doxorubicin acts as a redox cycler at the ETC (6, 25), mitochondria contain many other sources of ROS. Among those, we have characterized the relevant role of monoamine oxidases (MAOs) in several cardiac pathologies (17, 18, 34, 36). MAOs are located at the outer mitochondrial membrane, and exist in two different isoforms (*i.e.*, MAO-A and MAO-B), the crystal structures of which have been completely solved (7, 57). MAOs catalyze the deamination of biogenic amines that are relevant for cardiac function. The catalytic products are H_2O_2, aldehydes, and ammonia (17), which can synergize in inducing mitochondrial and cardiac dysfunction (34, 36). Besides these biochemical features, MAOs are the only mitochondrial sources of ROS that can be targeted by clinically available drugs (17). In addition, doxorubicin-induced neurotoxicity has been linked to an increase in MAO activity (49), and several cancerous tissues (*e.g.*, prostate cancer, Hodgkin's lymphomas) display a decrease in cell growth upon MAO inhibition alone (27) or in combination with doxorubicin treatment (39).

Chronic doxorubicin toxicity is well documented (21, 33, 44). However acute DC may occur during doxorubicin administration or immediately afterward in up to 40% of treated patients, leading to abnormal changes in the left ventricle (LV), cardiac rhythm disturbances, and alterations in cell metabolism (23, 48, 60). Here, we tested the hypothesis that a primary increase in mitochondrial ROS elicited by doxorubicin could be modulated by MAOs, thus leading to cardiac dysfunction. In particular, we investigated whether (i) MAOs are involved in mitochondrial ROS formation induced by doxorubicin; (ii) MAO-dependent oxidative stress triggered by doxorubicin can impair both mitochondrial and cell functions, eventually causing cardiomyocyte death; (iii) MAO inhibition can prevent doxorubicin-induced cardiotoxicity *in vivo*.

Results

MAO inhibition reduces mitochondrial oxidative stress induced by doxorubicin in cardiomyocytes

Despite the cardiotoxicity elicited by doxorubicin being well documented (10, 25, 69), the connection between this drug and the deleterious effects elicited by the elevation in mitochondrial ROS levels has been described mostly using supratherapeutic concentrations of doxorubicin (6). To verify that doxorubicin could increase ROS levels in neonatal rat ventricular myocytes (NRVMs), we treated cells with a clinically relevant concentration (6, 44, 62) of doxorubicin (*i.e.*, 0.5 μM) for 24 h. Moreover, to test possible involvement of MAOs, we incubated cells with 100 μM pargyline, a selective inhibitor of both MAO isoforms (18). Mitochondrial and cytosolic ROS levels were monitored using either MitoHyPer or Cyto-HyPer, genetically encoded sensors highly specific for H_2O_2 (4).

Doxorubicin-treated NRVMs displayed increased mitochondrial ROS levels that were totally prevented by pargyline (fluorescence ratio: untreated 2.30 ± 0.22; Doxo 3.12 ± 0.34; Doxo+Pargyline 2.14 ± 0.17; Fig. 1A). Of note, doxorubicin did not induce any increase in cytosolic ROS levels (Supplementary Fig. S1A). The pharmacological evidence was strengthened by a genetic approach. Indeed, in NRVMs knocked down (KD) for MAO-A (Supplementary Fig. S1B, full blot in Supplementary Fig. S2A) (18) mitochondrial ROS levels were reduced in the presence of doxorubicin (fluorescence ratio: scramble 2.90 ± 0.19; Doxo 3.44 ± 0.25; scramble+Doxo 2.89 ± 0.18; Fig. 1B). The protective efficacy of pargyline and the results obtained in MAO-A KD NRVMs demonstrate that MAOs can promote the formation of ROS caused by doxorubicin. This also implies that the redox cycling activity at the ETC results in the generation of a very limited amount of ROS, which becomes significant only when MAOs are involved.

Although DC attributed to excessive ROS production is well documented (44), the onset of cardiomyopathy in doxorubicin-treated patients may occur as a consequence of a further increase in ROS due to an additional event (*i.e.*, ischemia/reperfusion, exercise, infection) (1, 12), eventually leading to heart failure. To simulate the consequences derived from a secondary source of oxidative stress, NRVMs treated with 0.5 μM doxorubicin for 24 h, in the presence or absence of 100 μM pargyline, were further stimulated with increasing concentrations of exogenous H_2O_2. The coadministration of H_2O_2 (*i.e.*, 1–10–100 μM) with doxorubicin resulted in a further increase of mitochondrial ROS levels, which was prevented by MAO inhibition (fluorescence ratio after 10 μM H_2O_2: Untreated 4.06 ± 0.60; Doxo 6.60 ± 0.72; Doxo+Pargyline 3.41 ± 0.26; Fig. 1A). However, the protective effect of pargyline was lost when cells were exposed to 100 μM H_2O_2, probably due to the excessive oxidative stress and/or sensor saturation.

This result was strengthened by the genetic approach. Indeed, NRVMs KD for MAO-A cotreated with doxorubicin and H_2O_2 display decreased mitochondrial ROS levels compared with the scramble RNA-treated cells (fluorescence ratio after 10 μM H_2O_2: scramble 7.46 ± 0.40; Doxo 8.91 ± 0.56; scramble+Doxo 6.09 ± 0.65; Fig. 1B). Notably, cardiomyocytes incubated with doxorubicin and H_2O_2 displayed a severe increase of cytosolic ROS levels, which was not affected by MAO inhibition (Supplementary Fig. S1A). These results could suggest that the combination of MAO activation and doxorubicin may interfere with the mitochondrial antioxidant capacity leading to oxidative stress. To this aim, we monitored the intramitochondrial glutathione redox potential by means of Mito-Grx1-roGFP2, a genetically encoded sensor that detects changes in the mitochondrial ratio of oxidized to reduced glutathione (GSSG/GSH) (28). The coadministration of H_2O_2 (*i.e.*, 10–100 μM) with doxorubicin led to a dramatic increase in the GSSG/GSH ratio (fluorescence ratio after 100 μM H_2O_2: Untreated 0.25 ± 0.003; Doxo 0.28 ± 0.004; Fig. 1C), likely affecting the mitochondrial antioxidant capacity of NRVMs in these conditions. Importantly, MAO inhibition significantly preserved mitochondrial GSSG/GSH ratio (fluorescence ratio after 100 μM H_2O_2: Doxo+Pargyline 0.23 ± 0.004; Fig. 1C). A similar outcome was observed when the glutathione redox potential was monitored in the whole cell (Supplementary Fig. S1C), although the total thiol oxidation state was not affected by doxorubicin (Supplementary Fig. S1D). Since MAO inhibition prevented the rise in the mitochondrial/cell GSSG/GSH ratio without affecting cytosolic H_2O_2 levels, it is plausible that a secondary source of ROS [*e.g.*, NAD(P)H oxidases] is also at play here and that the excessive increase in H_2O_2-derived ROS levels in the cytosol was not correlated with MAO activity.

To strengthen the significance of the results obtained in NRVMs, we tested our hypothesis also in adult mouse ventricular myocytes (AMVMs). Of note, besides a more mature metabolic phenotype (*i.e.*, high dependency on fatty acid oxidation), AMVMs express prevalently MAO-B, while NRVMs contain mostly MAO-A (34). Since AMVMs are stable in cell culture for only up to 2 days, making the transfection of the cells with a sensor such as Mito-HyPer impossible, mitochondrial ROS levels were monitored by the reduced form of MitoTracker Red (MTR) (16).

AMVMs incubated with 0.5 μM doxorubicin for 24 h displayed an increase in mitochondrial ROS levels (Untreated 100% ± 11.08%; Doxo 154.74% ± 2.51%; Fig. 1D), which were further elevated by different concentrations of H_2O_2 (*i.e.*, 1–10 μM) (Fig. 1D). Similarly to what observed in NRVMs, the rise in mitochondrial ROS levels was prevented by treatment with 200 μM pargyline (after 10 μM H_2O_2: Untreated 178.79% ± 4.55%; Doxo 212.24% ± 12.69%; Doxo+Pargyline 157.82% ± 25.14%; Fig. 1D). Although after treatment with 100 μM H_2O_2 mitochondrial ROS could not be measured by MTR due to mitochondrial depolarization (18), pargyline was still protective. Indeed, the cotreatment with doxorubicin and H_2O_2 led to the transformation of rod-shaped cells into rounded dysfunctional cardiomyocytes. Conversely, pargyline treatment maintained the rod-shaped morphology of AMVMs (Supplementary Fig. S1E). These results demonstrate that the oxidative stress elicited by doxorubicin alone or by the cotreatment with doxorubicin and H_2O_2 is exacerbated by MAOs that act as ROS enhancers in cardiomyocytes.

To understand how doxorubicin treatment resulted in an increased MAO-dependent ROS formation, we evaluated MAO expression levels in both NRVMs and AMVMs. After 24 h of treatment with doxorubicin, both MAO-A in NRVMs and MAO-B in AMVMs expression levels were comparable

FIG. 1. Effects of doxorubicin and MAO inhibition on mitochondrial oxidative status. NRVMs have been treated with 0.5 μM doxorubicin for 24 h, in the presence or absence of 100 μM pargyline. AMVMs have been treated with 0.5 μM doxorubicin for 24 h, in the presence or absence of 200 μM pargyline. Cells have been further stimulated with increasing concentrations of H_2O_2 (*i.e.*, 1–10–100 μM) for 10 min. **(A)** Mitochondrial H_2O_2 formation measured by Mito-HyPer in isolated NRVMs. $^{*}p < 0.001$ *versus* Untreated, $^{\#}p < 0.001$ *versus* Doxo, $^{\$}p < 0.001$ *versus* Basal Untreated by one-way ANOVA with *post hoc* Tukey's multiple comparison test. **(B)** Mitochondrial H_2O_2 formation measured by Mito-HyPer in isolated NRVMs. Cells have been previously transfected with scramble or MAO-A siRNA. $^{*}p < 0.05$ *versus* Scramble, $^{\#}p < 0.01$ *versus* Scramble+Doxo, $^{\varsigma}p < 0.01$ *versus* Scramble, $^{\S}p < 0.001$ *versus* Scramble+Doxo, $^{\$}p < 0.001$ *versus* Scramble Basal by one-way ANOVA with *post hoc* Tukey's multiple comparison test. **(C)** Mitochondrial GSSG/GSH ratio measured by Mito-Grx1-roGFP in isolated NRVMs. $^{*}p < 0.01$ *versus* Untreated, $^{\#}p < 0.01$ *versus* Doxo, $^{\varsigma}p < 0.001$ *versus* Doxo, $^{\S}p < 0.05$ *versus* Untreated, $^{£}p < 0.05$ *versus* Basal Untreated, $^{\$}p < 0.001$ *versus* Basal Untreated by one-way ANOVA with *post hoc* Tukey's multiple comparison test. **(D)** Mitochondrial ROS formation measured by MTR in AMVMs. $^{*}p < 0.05$ *versus* Untreated, $^{\#}p < 0.05$ *versus* Doxo, $^{\S}p < 0.05$ *versus* Basal Doxo, $^{\varsigma}p < 0.01$ *versus* Basal Untreated, $^{\$}p < 0.001$ *versus* Basal Untreated by one-way ANOVA with *post hoc* Tukey's multiple comparison test. Approximately 30 cells were analyzed per condition in each experiment, and all the experiments were performed at least three times using three different animal or cell preparations. Data are expressed as mean ± SEM. AMVM, adult mouse ventricular myocyte; GSSG/GSH, glutathione disulfide/glutathione; MAO, monoamine oxidase; MTR, MitoTracker Red; NRVM, neonatal rat ventricular myocyte; ROS, reactive oxygen species; SEM, standard error of the mean.

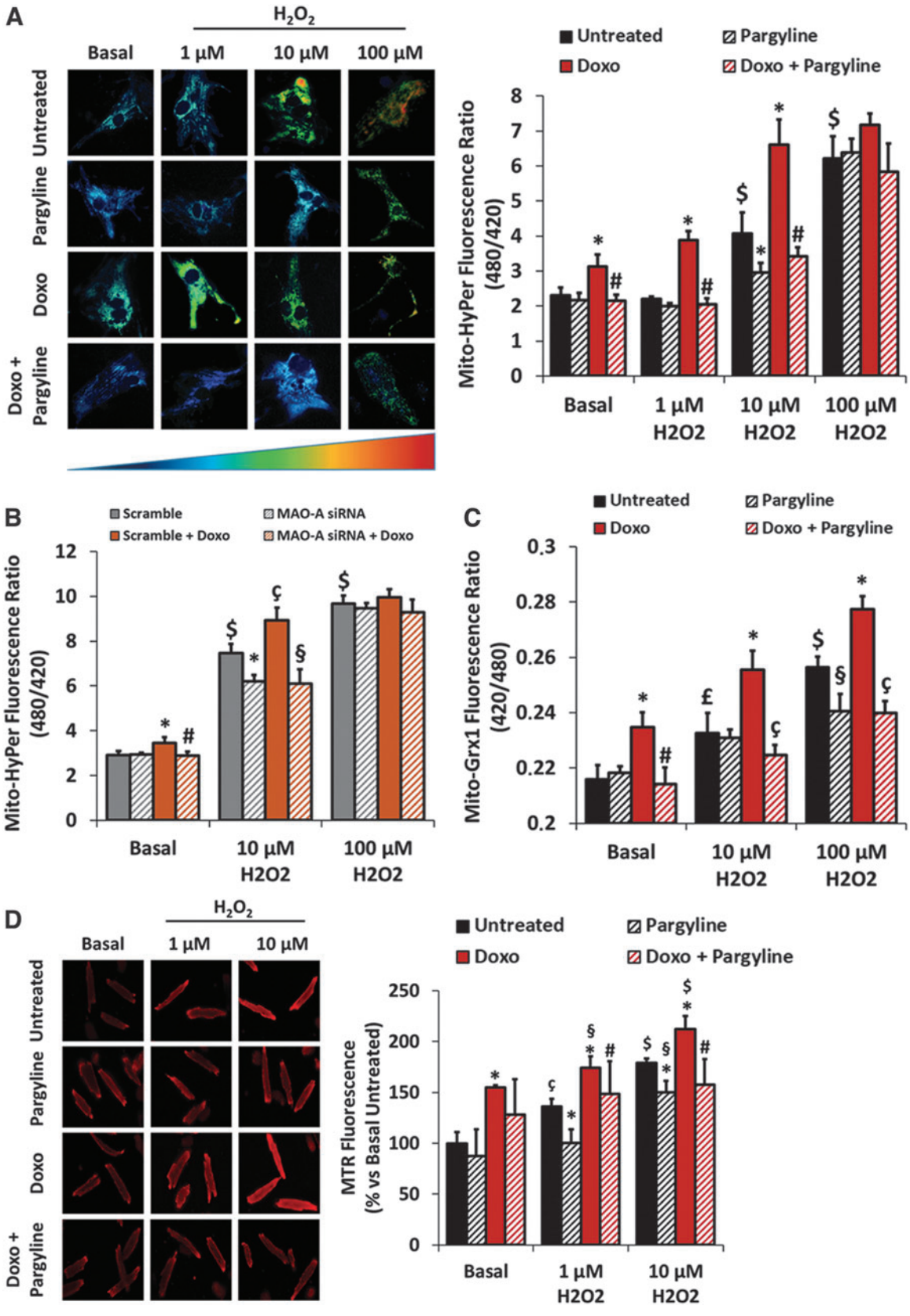
A
H_2O_2
Basal
1 µM
10 µM
100 µM
Untreated
Pargyline
Doxo
Doxo + Pargyline
Mito-HyPer Fluorescence Ratio (480/420)
Basal
1 µM H2O2
10 µM H2O2
100 µM H2O2
B
Scramble
MAO-A siRNA
Scramble + Doxo
MAO-A siRNA + Doxo
Mito-HyPer Fluorescence Ratio (480/420)
C
Mito-Grx1 Fluorescence Ratio (420/480)
D
MTR Fluorescence (% vs Basal Untreated)

with the untreated control (Supplementary Fig. S1F, G, full blots shown in Supplementary Fig. S2B, C). Hence, we investigated whether doxorubicin treatment could increase MAO activity in NRVMs. H_2O_2 formation was monitored by means of Mito-HyPer in cells pretreated with 0.5 μM doxorubicin for 24 h, in the presence or absence of 100 μM pargyline, and then incubated with 20 μM of the MAO substrate tyramine for 2 h. Treatment with tyramine significantly increased H_2O_2 levels within mitochondria (Supplementary Fig. S1H), while the cotreatment with tyramine and doxorubicin did not induce any further increase (Supplementary Fig. S1H). In both cases, MAO inhibition completely prevented this increase in H_2O_2 formation. This result suggests that, when the MAO enzyme is working at its maximum (*i.e.*, in the presence of its substrate tyramine), doxorubicin cannot further enhance MAO-dependent ROS generation.

MAO inhibition ameliorates both mitochondrial function and morphology altered by cotreatment with doxorubicin and H_2O_2 in cardiomyocytes

The increase in mitochondrial ROS production causes mitochondrial dysfunction, characterized by mitochondrial depolarization (37). Hence, we monitored mitochondrial membrane potential ($\Delta\Psi m$) using tetramethylrhodamine (TMRM). NRVMs treated with 0.5 μM doxorubicin for 24 h displayed a decrease in $\Delta\Psi m$ that was partially prevented by MAO inhibition (F/F_{FCCP}: Untreated 3.49 ± 0.14; Doxo 2.34 ± 0.10; Doxo+Pargyline 3.08 ± 0.11; Fig. 2A).

Subsequently, doxorubicin-treated cells were coincubated with increasing concentrations of exogenous H_2O_2 (*i.e.*, 10–100 μM), and $\Delta\Psi m$ was monitored up to 2 h after the treatment, in the presence or absence of 100 μM pargyline. H_2O_2 induced a progressive decrease in $\Delta\Psi m$, which was exacerbated by the presence of doxorubicin (Fig. 2B). This effect was prevented by pargyline, and the protection was observed even 2 h after the addition of 100 μM H_2O_2, both in control and in doxorubicin-treated cells (after 2 h: Untreated $30.56\% \pm 1.59\%$; Doxo $6.96\% \pm 1.63\%$; Doxo+Pargyline $56.20\% \pm 7.40\%$; Fig. 2B).

It has been reported that doxorubicin-derived ROS can sensitize the propensity for the mitochondrial permeability transition pore (PTP) to open (14). Thus, we treated NRVMs with 0.5 μM doxorubicin, in the presence or absence of 100 μM pargyline, and monitored the opening of the PTP using the calcein assay (50). After triggering the PTP opening by means of the Ca^{2+} ionophore calcimycin, doxorubicin-treated NRVMs displayed a gradual increase in PTP opening compared with the control, an effect that was prevented by MAO inhibition (after 300 s: Untreated $74.86\% \pm 3.71\%$; Doxo $50.06\% \pm 6.89\%$; Doxo+Pargyline $82.99\% \pm 6.56\%$; Fig. 2C).

Since lipid peroxidation is one of the downstream effects of an increase in ROS levels induced by doxorubicin (44), we assessed malondialdehyde (MDA) production in NRVMs (Supplementary Fig. S3A) (67, 72). Cells treated for 24 h with 0.5 μM doxorubicin displayed a significant increase in MDA production compared with the control (Fluorescence/mg protein normalized to control: Untreated 1 ± 0.03, Doxo 1.43 ± 0.04; Fig. 2D). Notably, the inhibition of MAO by pargyline reduced doxorubicin-induced lipid peroxidation (Fluorescence/mg protein normalized to control: Doxo+Pargyline 1.09 ± 0.10; Fig. 2D). Therefore, doxorubicin-induced mitochondrial dysfunction and lipid peroxidation require MAO involvement, whereas doxorubicin *per se* (*i.e.*, in the presence of MAO inhibition) causes only a slight impairment of mitochondria.

Alterations in mitochondrial bioenergetics induced by an increase in mitochondrial ROS are associated with alterations in the structure of mitochondria (5). Thus, mitochondrial morphology was analyzed by conventional transmission electron microscopy (TEM) in NRVMs treated with 0.5 μM doxorubicin for 24 h, with 10 μM H_2O_2 for 1 h, in the presence or absence of 100 μM pargyline. Doxorubicin-treated cardiomyocytes displayed mitochondria with highly reduced size and irregular shape (Fig. 3A), confirming a previous report (73). Mitochondrial morphological alterations were further supported by the analysis of mitochondrial perimeter, which was reduced in doxorubicin-treated cells, in a process prevented by pargyline (Fig. 3B).

The TEM analysis was paralleled by confocal microscopy. To this aim, NRVMs were treated as described above (*i.e.*, 0.5 μM doxorubicin; 10 μM H_2O_2; 100 μM pargyline), and mitochondria were stained for TOM20. Doxorubicin or H_2O_2 alone did not affect mitochondrial distribution (Fig. 4A), while their combination induced the disruption of the mitochondrial network (Fig. 4A). The alteration in mitochondrial distribution was validated by quantitative analysis expressed by the *R* parameter (59), defined as the ratio between average and maximal fluorescence on a given cell. The distribution of this parameter was significantly decreased in NRVMs incubated with both doxorubicin and H_2O_2, while it was restored by the treatment with pargyline (Fig. 4B), reflecting a decrease in dysfunctional mitochondria (*R* value: Untreated 0.165 ± 0.004; Doxo+H_2O_2 0.114 ± 0.003; Doxo+H_2O_2+Pargyline 0.141 ± 0.004; Supplementary Fig. S3B).

These data demonstrate that MAO inhibition prevents the alterations of mitochondrial bioenergetics and morphology in NRVMs treated with doxorubicin and subjected to an additional stress induced by exogenous H_2O_2.

MAO inhibition ameliorates cardiomyocyte contractility altered by doxorubicin-induced oxidative stress

Besides mitochondria, doxorubicin has been reported to alter the entire ultrastructure of cardiomyocytes (61). Therefore, we investigated whether treatment with pargyline could prevent doxorubicin-induced derangement of sarcomeric organization in cardiomyocytes. NRVMs were incubated with 0.5 μM doxorubicin for 24 h, in the presence or absence of 100 μM pargyline, and subsequently treated with 10 μM H_2O_2 for 1 h. The distribution of the α-sarcomeric actinin was evaluated by immunocytochemistry. Similarly to what was observed with mitochondrial morphology, doxorubicin or H_2O_2 alone was not sufficient to modify sarcomeric structure (Fig. 4C), while their combination altered the distribution of the α-sarcomeric actinin in cardiomyocytes (Fig. 4C, D). In contrast, NRVMs pretreated with pargyline displayed a distribution of the α-sarcomeric actinin similar to control, indicating a well-aligned sarcomeric pattern (Fig. 4C, D).

In respect to the excitation–contraction (EC) coupling (66) and in parallel with the evaluation of morphological alteration in cardiomyocytes, we analyzed doxorubicin-derived changes in intracellular $[Ca^{2+}]$ homeostasis.

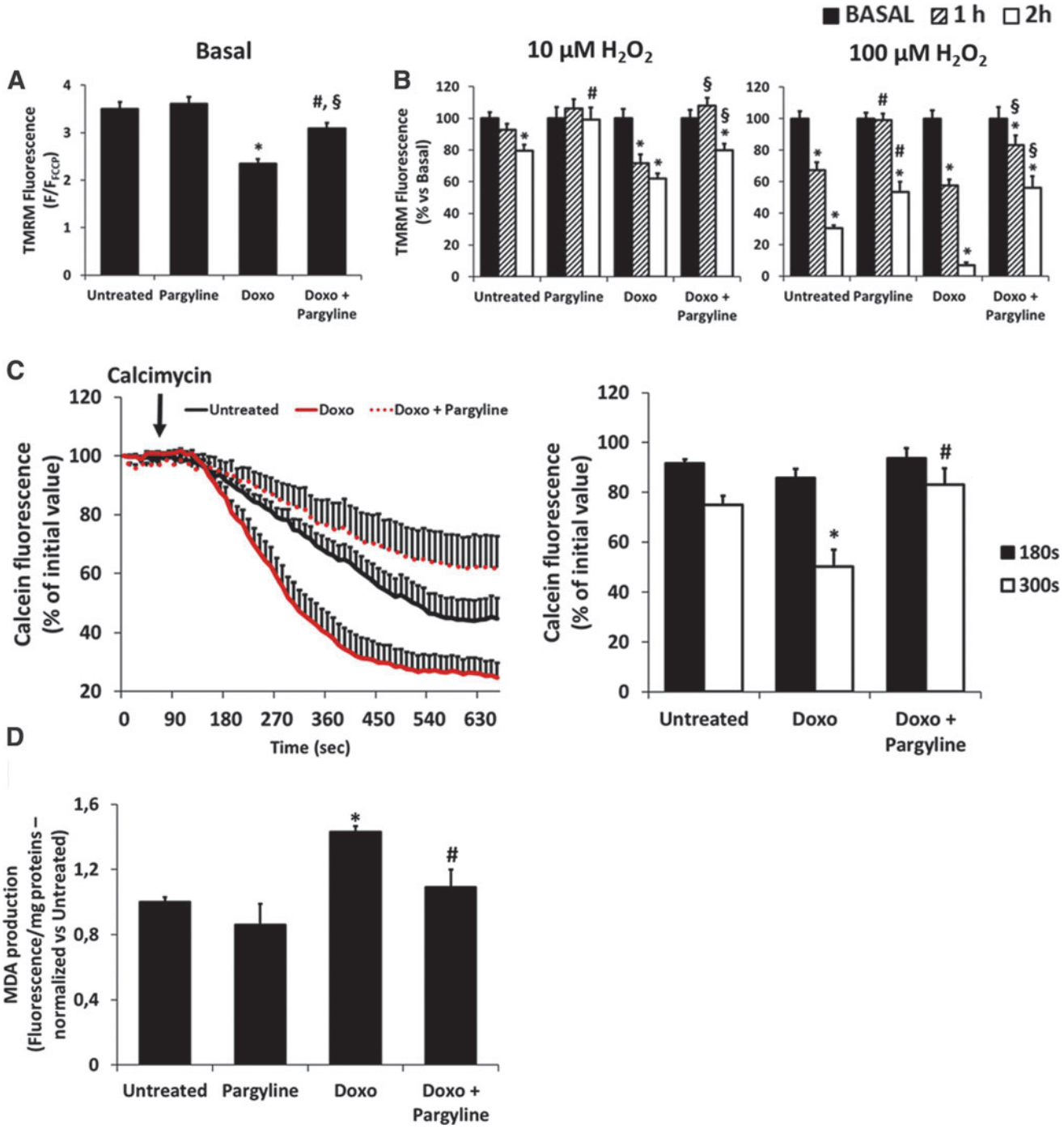

FIG. 2. Effects of doxorubicin and MAO inhibition on mitochondrial function and lipid peroxidation. NRVMs have been treated with 0.5 μM doxorubicin for 24 h, in the presence or absence of 100 μM pargyline. **(A)** $\Delta\Psi$m monitored by TMRM fluorescence in isolated NRVMs. TMRM fluorescence was normalized using 5 μM FCCP. $^{*}p < 0.001$ *versus* Untreated, $^{\S}p < 0.05$ *versus* Untreated, $^{\#}p < 0.001$ *versus* Doxo by one-way ANOVA with *post hoc* Tukey's multiple comparison test. **(B)** $\Delta\Psi$m monitored by TMRM fluorescence in isolated NRVMs. TMRM fluorescence was evaluated before and after 1 and 2 h of treatment with increasing concentrations of H_2O_2 (*i.e.*, 10–100 μM). TMRM fluorescence was normalized using 5 μM FCCP. $^{*}p < 0.001$ *versus* Basal, $^{\#}p < 0.001$ *versus* Untreated, $^{\S}p < 0.001$ *versus* Doxo by one-way ANOVA with *post hoc* Tukey's multiple comparison test. **(C)** PTP opening monitored by decrease of calcein fluorescence in isolated NRVMs. PTP opening was triggered by 5 μM calcimycin. Data were quantified after 180 and 300 s from the beginning of the experiment. $^{*}p < 0.001$ *versus* Untreated, $^{\#}p < 0.01$ *versus* Doxo by one-way ANOVA with *post hoc* Tukey's multiple comparison test. **(D)** MDA formation in isolated NRVMs. Raw fluorescence values were normalized to milligram proteins, and then normalized *versus* Untreated. $^{*}p < 0.01$ *versus* Untreated, $^{\#}p < 0.05$ *versus* Doxo by one-way ANOVA with *post hoc* Tukey's multiple comparison test. Approximately 30 cells were analyzed per condition in each experiment, and all the experiments were performed three times using three different animal preparations. MDA assay was performed three times using three different animal preparations. Data are expressed as mean ± SEM. $\Delta\Psi$m, mitochondrial membrane potential; FCCP, carbonyl cyanide-p-trifluoromethoxyphenylhydrazone; MDA, malondialdehyde; PTP, permeability transition pore; TMRM, tetramethylrhodamine.

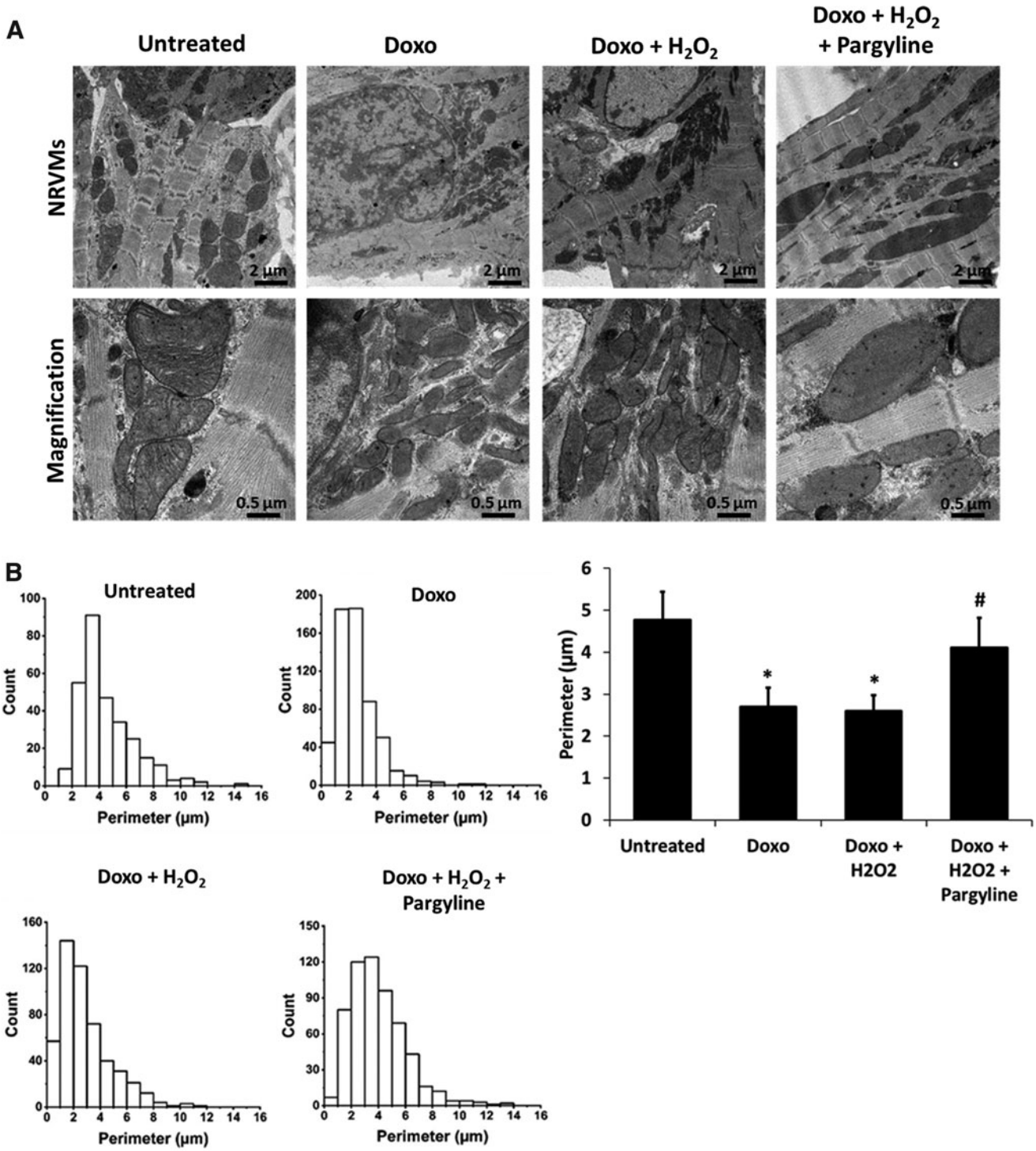

FIG. 3. Effects of doxorubicin and MAO inhibition on mitochondrial morphology. (A) TEM of isolated NRVMs treated with 0.5 μM doxorubicin for 24 h, in the presence or absence of 100 μM pargyline. Cells have been further stimulated with 10 μM H_2O_2 for 1 h. **(B)** Probability histograms of mitochondrial perimeter, representing values count on the *y axis* and mitochondrial perimeter values on the *x* axis. The bar graph displays the average of the mitochondrial perimeter. $^{*}p < 0.001$ *versus* Untreated, $^{\#}p < 0.01$ *versus* Doxo+H_2O_2 by one-way ANOVA with *post hoc* Tukey's multiple comparison test. Where data were not normally distributed, the Kruskal–Wallis test has been applied. All the experiments were performed three times using three different animal preparations. Untreated: $N = 15$ cells, 297 mitochondria. Doxo: $N = 14$ cells, 588 mitochondria. Doxo+H_2O_2: $N = 11$ cells, 463 mitochondria. Doxo+H_2O_2+pargyline: $N = 15$ cells, 536 mitochondria. Data are expressed as mean ± SEM. TEM, transmission electron microscopy.

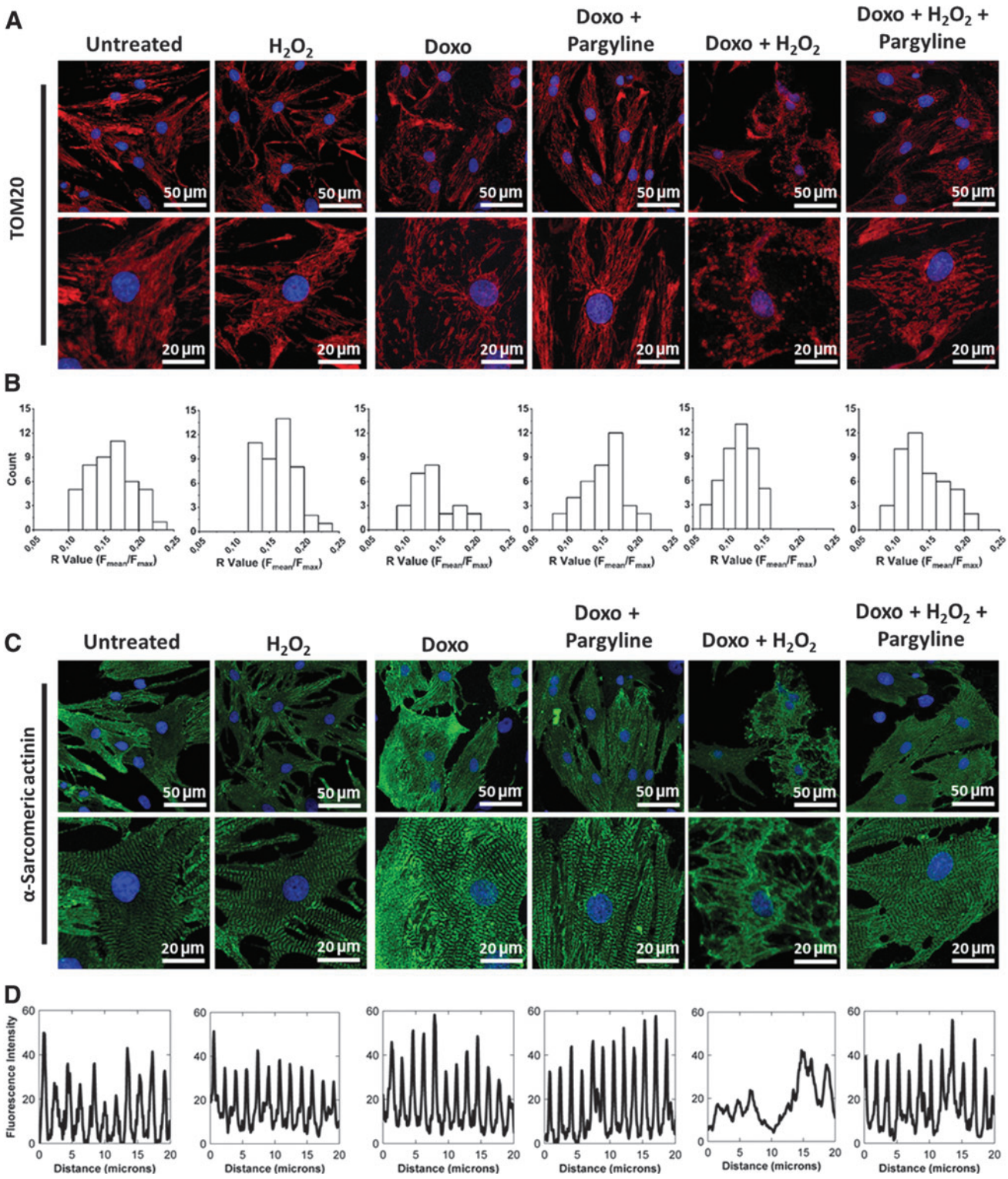

FIG. 4. Effects of doxorubicin and MAO inhibition on mitochondria and sarcomere alignment. NRVMs have been treated with 0.5 μM doxorubicin for 24 h, in the presence or absence of 100 μM pargyline. Cells have been further stimulated with 10 μM H_2O_2 for 1 h. **(A)** Mitochondrial morphology assessed by confocal microscopy in isolated NRVMs. Confocal images were processed for immunofluorescent labeling of TOM20 (*red*), while nuclei were stained with DAPI (*blue*). Both representative images (*upper row*) and regions of interests (*lower row*) are provided. **(B)** Probability histograms of mitochondrial distribution, representing values count on the *y* axis and *R* values on the *x* axis. **(C)** Sarcomere arrangement assessed by confocal microscopy in isolated NRVMs. Confocal images were processed for immunofluorescent labeling of α-sarcomeric actinin (*green*), while nuclei were stained with DAPI (*blue*). Both representative images (*upper row*) and regions of interests (*lower row*) are provided. **(D)** The fluorescence intensity of the α-sarcomeric actinin was plotted and reported on the graph to show the effect of the treatments on the distribution of the sarcomeres within the cell. Approximately 30 cells were analyzed per condition in each experiment, and all the experiments were performed at least three times using three different animal preparations.

NRVMs were treated with 0.5 μM doxorubicin for 24 h in the presence or absence of 100 μM pargyline, and intracellular [Ca^{2+}] transients were monitored by means of Fluo-4 fluorescence. Doxorubicin did not induce significant changes in transient amplitude, while it increased transient frequency, which was prevented by pargyline (Untreated 100% ± 8.90%, Doxo 138.34% ± 5.18%, Doxo+Pargyline 87.93% ± 10.76%; Fig. 5A, B). In addition, we evaluated sarcoplasmic reticulum (SR) Ca^{2+} content by stimulating the release of Ca^{2+} from the SR using 10 mM caffeine. Doxorubicin-treated cardiomyocytes displayed a decrease in response to caffeine (Untreated 100% ± 4.68%, Doxo 73.80% ± 10.12%, Doxo+Pargyline 94.11% ± 6.58%; Fig. 5A, C) and an increase in the fractional release of Ca^{2+} (Untreated 46.93% ± 3.80%, Doxo 56.59% ± 3.59%, Doxo+Pargyline 44.68% ± 6.63%; Fig. 5C). Similar results were obtained by Sag *et al.* (53). Their interpretation of this phenomenon was that an increase in both NCX activity and RyR_2 opening would lead to an increase of trans-sarcolemmal Ca^{2+} extrusion, and to SR Ca^{2+} leak. Of note, the doxorubicin-dependent SR Ca^{2+} load reduction was prevented by MAO inhibition (Fig. 5C).

To further investigate SR function and Ca^{2+} cycling, the response to caffeine was monitored in isoproterenol-treated NRVMs. Doxorubicin is reported to alter the regulation of β-adrenergic receptors (22), thereby worsening the latent DC. Administration of isoproterenol increases mitochondrial ROS levels (51), allowing us to further investigate the effect elicited by pargyline. Doxorubicin-treated cardiomyocytes incubated with 10 μM isoproterenol for 15 min did not recover the spontaneous beating activity after caffeine (Fig. 5A). Conversely, MAO inhibition resulted in the recovery of Ca^{2+} transients after caffeine (Fig. 5A–D).

Taken together, these data demonstrate that pargyline prevents doxorubicin-induced derangement in EC coupling by preserving both cardiomyocyte structure and intracellular [Ca^{2+}] homeostasis. Moreover, the protection against doxorubicin-induced oxidative stress is maintained even in the presence of an additional stress, such as exogenous H_2O_2 or β-adrenergic stimulation.

MAO inhibition reduces cell death induced by doxorubicin and oxidative stress in cardiomyocytes

A severe oxidative stress results in cell death in any pathological condition, including DC (21). It has been reported that doxorubicin-induced mitochondrial dysfunction and oxidative stress could synergize in promoting apoptosis (37). To test whether MAO inhibition affects this process, NRVMs were treated with 0.5 μM doxorubicin, in the presence or absence of 100 μM pargyline, and stained with Annexin-V-Fluos that recognizes exposed phosphatidylserines, a typical feature of apoptosis (Supplementary Fig. S3C) (13). Doxorubicin induced a marked increase in Annexin-V positive cells, which was prevented by pargyline treatment (Untreated 6.84% ± 1.06%, Doxo 26.90% ± 4.41%, Doxo+Pargyline 9.79% ± 0.43%; Fig. 6A). In addition, we wondered whether autophagy processes could be involved. At baseline, LC3B-II and p62 levels were not significantly different between the groups (Supplementary Fig. S3D, E, full blots in Supplementary Fig. S2D, E). Upon inhibition of lysosomal degradation, LC3B-II abundance increased to the same extent in control *versus* doxorubicin-treated cells (Supplementary Fig. S3D), suggesting that autophagy levels and autophagic flux were not affected by the 24 h-long 0.5 μM doxorubicin treatment. Thus, doxorubicin-induced alterations in our model appear to occur independently of autophagy.

Since the induction of apoptosis induced by doxorubicin might be upstream of the rupture of cell membrane, leading to necrosis, we investigated whether pargyline could decrease doxorubicin-induced cell death in cardiomyocytes. NRVMs were treated with 0.5 μM doxorubicin for 24 h, in the presence or absence of 100 μM pargyline, and cell death was monitored by lactic dehydrogenase (LDH) release after the administration of different concentrations of H_2O_2 (*i.e.*, 10–100 μM). H_2O_2 *per se* induced a dose-dependent increase in cell death in NRVMs (after 6 h*:* 73.88% ± 1.82% with 10 μM H_2O_2, 80.89% ± 1.44% with 100 μM H_2O_2; Fig. 6B, C), which was prevented by pargyline (after 6 h: 33.37% ± 5.23% with 10 μM H_2O_2, 61.61% ± 7.74% with 100 μM H_2O_2; Fig. 6B, C). The injury elicited by H_2O_2 was accelerated in the presence of doxorubicin, with cell death occurring after only 1 h of treatment (after 1 h: 54.51% ± 5.55% with 10 μM H_2O_2; after 3 h: 73.94% ± 5.05% with 10 μM H_2O_2; Fig. 6B, C). Notably, pargyline reduced significantly the extent of cell death in doxorubicin-treated NRVMs, in the presence of either 10 μM H_2O_2 (after 1 h: 4.53% ± 2.03%; after 3 h: 27.77% ± 1.08%, Fig. 6B) or 100 μM H_2O_2 (after 1 h: 6.85% ± 2.22%; after 3 h: 42.70% ± 3.11%, Fig. 6C). However, the protection by pargyline against cell death was not observed when the exposure to oxidative stress was massive (*i.e.*, treatment with doxorubicin and 6 h of exposure to 100 μM H_2O_2) (Fig. 6C).

Taken together, these results demonstrate the protective effect elicited by MAO inhibition in cardiomyocytes coincubated with doxorubicin and H_2O_2.

FIG. 5. Effects of doxorubicin and MAO inhibition on cytosolic [Ca^{2+}] homeostasis. NRVMs have been treated with 0.5 μM doxorubicin for 24 h, in the presence or absence of 100 μM pargyline. Cytosolic [Ca^{2+}] transients have been monitored by Fluo-4 AM. **(A)** Representative intracellular [Ca^{2+}] transients, intracellular [Ca^{2+}] peaks after stimulation with 10 mM caffeine, and intracellular [Ca^{2+}] transients after cotreatment with 10 mM caffeine and 10 μM isoproterenol. **(B)** Transient amplitude and transient frequency average in spontaneous beating NRVMs. $*p < 0.05$ *versus* Untreated, $^{\#}p < 0.01$ *versus* Doxo by one-way ANOVA with *post hoc* Tukey's multiple comparison test. **(C)** Caffeine peak average and SR fractional release of Ca^{2+} in spontaneous beating NRVMs. $*p < 0.05$ *versus* Untreated, $^{\#}p < 0.05$ *versus* Doxo by one-way ANOVA with *post hoc* Tukey's multiple comparison test. **(D)** Transient amplitude and transient frequency average in the presence of isoproterenol, before and after caffeine stimulus. $*p < 0.05$ *versus* before caffeine, $^{\#}p < 0.001$ *versus* before caffeine by one-way ANOVA with *post hoc* Tukey's multiple comparison test. Approximately 30 cells were analyzed per condition in each experiment, and all the experiments were performed three times using three different animal preparations. Data are expressed as mean ± SEM. AM, acetoxymethyl; SR, sarcoplasmic reticulum.

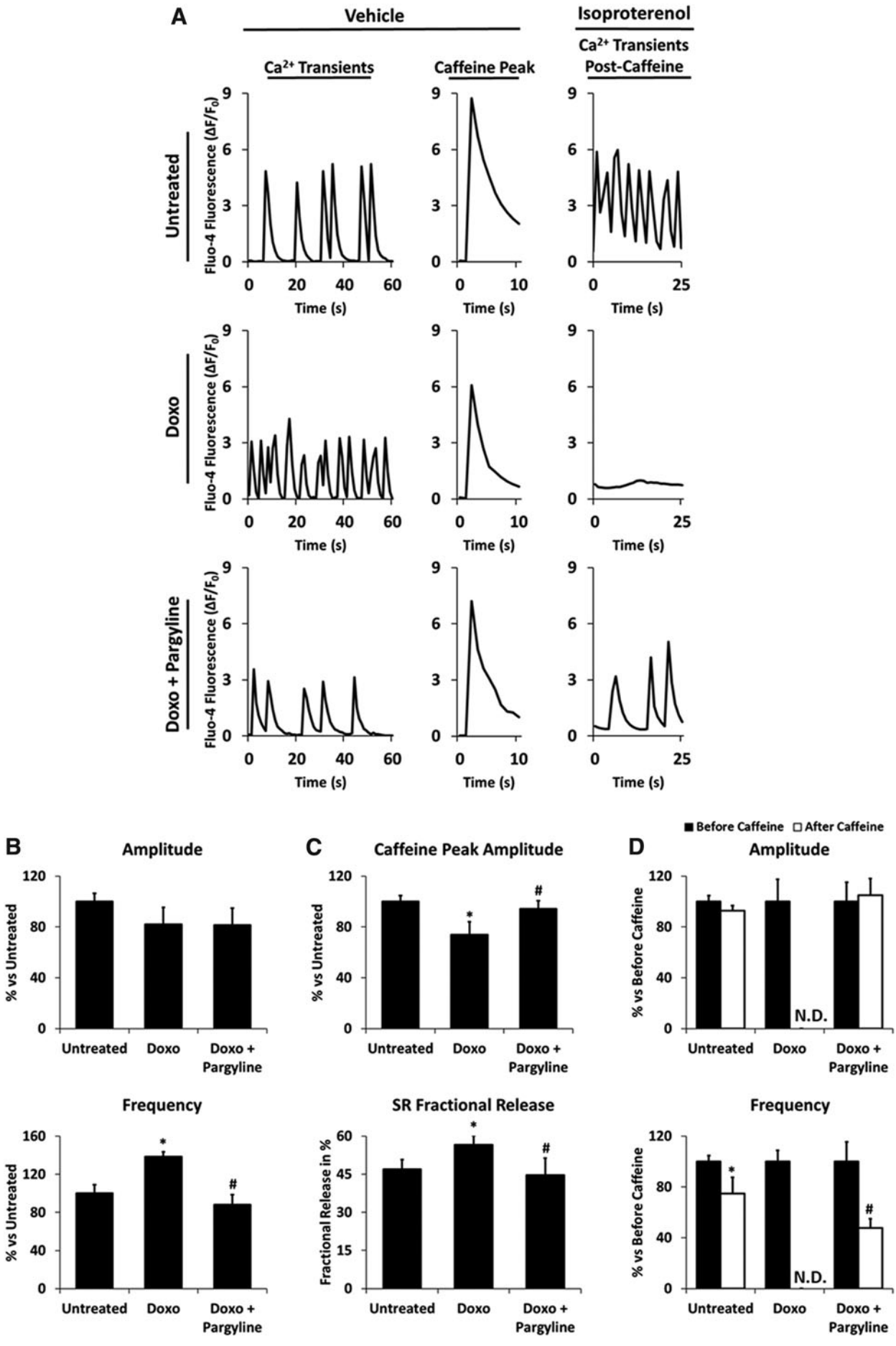
A
Vehicle
Isoproterenol
Ca2+ Transients
Caffeine Peak
Ca2+ Transients Post-Caffeine
Untreated
Doxo
Doxo + Pargyline
Fluo-4 Fluorescence (ΔF/F0)
Time (s)
B
Amplitude
% vs Untreated
Frequency
C
Caffeine Peak Amplitude
SR Fractional Release
Fractional Release in %
D
Before Caffeine
After Caffeine
% vs Before Caffeine
N.D.
Untreated
Doxo
Doxo + Pargyline

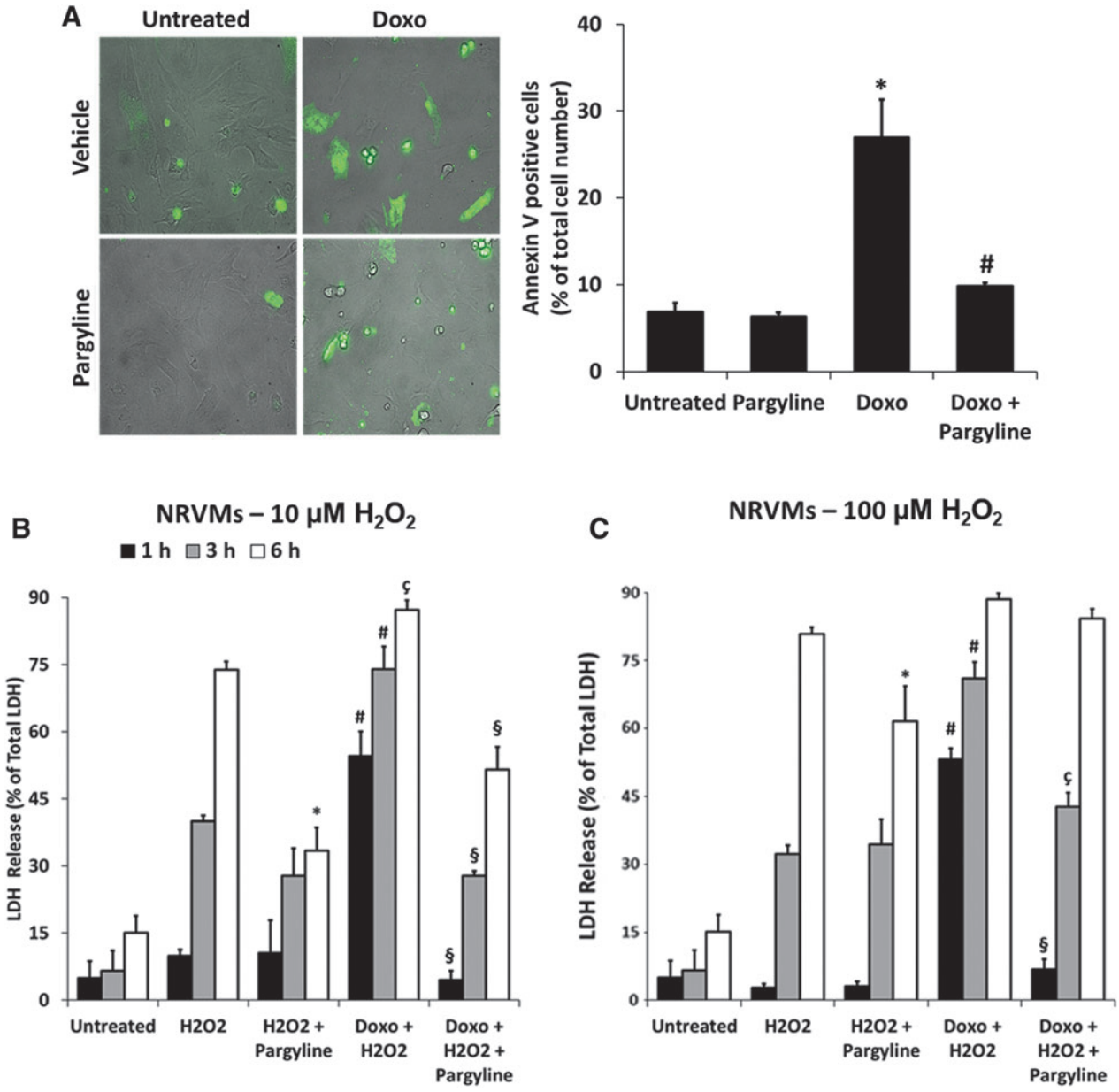

FIG. 6. Effects of doxorubicin and MAO inhibition on cardiomyocyte viability. NRVMs have been treated with 0.5 μM doxorubicin for 24 h, in the presence or absence of 100 μM pargyline. **(A)** Apoptosis evaluated by Annexin-V-Fluos staining in isolated NRVMs. Histogram displays the percentage of Annexin V-positive cells normalized to the total number of cells identified by bright-field images. $^{*}p < 0.01$ *versus* Untreated, $^{\#}p < 0.01$ *versus* Doxo by the Kruskal–Wallis test. **(B)** Cell death measured by LDH release from isolated NRVMs. Cells have been further stimulated with 10 μM H_2O_2, and supernatants were collected at different time points. $^{*}p < 0.001$ *versus* H_2O_2; $^{\#}p < 0.001$ *versus* H_2O_2; $^{\varsigma}p < 0.01$ *versus* H_2O_2; $^{\S}p < 0.001$ *versus* Doxo+H_2O_2 by one-way ANOVA with *post hoc* Tukey's multiple comparison test. **(C)** Cell death measured by LDH release from isolated NRVMs. Cells have been further stimulated with 100 μM H_2O_2, and supernatants were collected at different time points. $^{*}p < 0.05$ *versus* H_2O_2; $^{\#}p < 0.001$ *versus* H_2O_2; $^{\S}p < 0.001$ *versus* Doxo+H_2O_2; $^{\varsigma}p < 0.01$ *versus* Doxo+H_2O_2 by one-way ANOVA with *post hoc* Tukey's multiple comparison test. For the evaluation of apoptosis, ~100 cells were analyzed per condition in each experiment, and all the experiments were performed three times using three different animal preparations. For LDH release approximately three to four wells were analyzed per condition in each experiment. All the experiments were performed at least three times using three different animal preparations. Data are expressed as mean ± SEM. LDH, lactic dehydrogenase.

MAO inhibition prevents LV dilation and dysfunction in doxorubicin-treated mice

Given the protective effect exerted by MAO inhibition against doxorubicin-induced cellular derangements and death *in vitro*, we next investigated whether pharmacological MAO inhibition could protect against doxorubicin-induced cardiotoxicity *in vivo*. To this aim, mice were injected with doxorubicin and immediately randomized to receive either vehicle or pargyline. LV function was monitored by echocardiography.

After 5 weeks, doxorubicin-treated mice exhibited no change in LV dimension in end-diastole (Fig. 7A), but

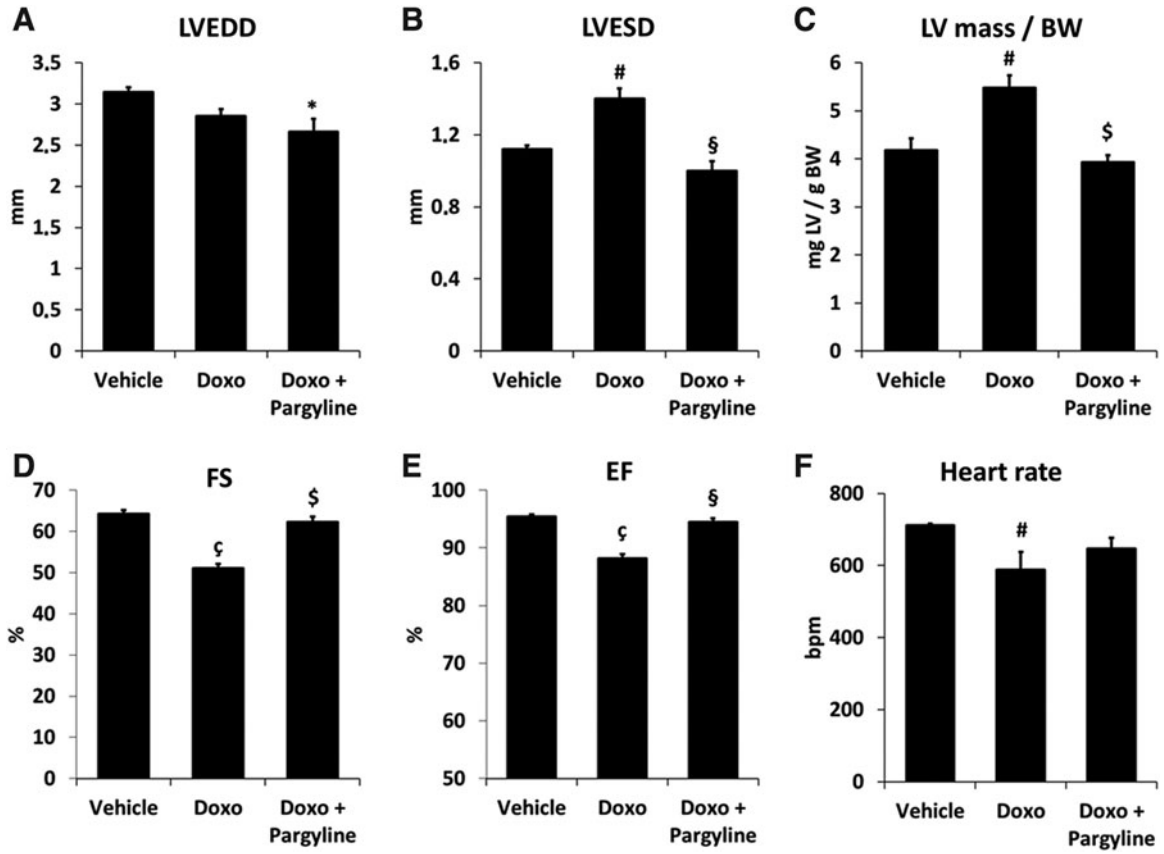

FIG. 7. Changes in cardiac morphology and function in doxorubicin-treated mice. (A–C) Changes in cardiac morphology and **(D–F)** function in vehicle- ($n=5$), doxorubicin- ($n=7$), and doxorubicin and pargyline-treated mice ($n=5$). $^{*}p<0.05$, $^{\#}p<0.01$, $^{ç}p<0.001$ *versus* Vehicle; $^{\S}p<0.01$, $^{\$}p<0.001$ *versus* Doxo by one-way ANOVA with *post hoc* Tukey's multiple comparison test. Where data were not normally distributed, the Kruskal–Wallis test has been applied. Data are expressed as mean ± SEM. EF, ejection fraction; FS, fractional shortening; LV mass/BW, left ventricle mass/body weight; LVEDD, left ventricular end-diastolic dimension; LVESD, left ventricular end-systolic dimension.

TABLE 1. CHANGES IN CARDIAC MORPHOLOGY AND *IN VIVO* VENTRICULAR FUNCTION INDUCED BY DOXORUBICIN IN VEHICLE- AND PARGYLINE-TREATED MICE

	Vehicle	*Doxo*	*Doxo+Pargyline*
BW, g	31.40 ± 0.47	22.38 ± 0.91[a]	24.28 ± 1.20[a]
LV mass/BW	4.18 ± 0.25	5.48 ± 0.26[b]	3.93 ± 0.15[c]
IVS, cm	0.96 ± 0.02	1.02 ± 0.03	0.94 ± 0.04
LVEDD, cm	3.14 ± 0.06	2.85 ± 0.09	2.66 ± 0.16[d]
LVESD, cm	1.12 ± 0.02	1.40 ± 0.05[b]	1.00 ± 0.05[c]
LVPW, cm	0.9 ± 0.03	1.01 ± 0.03[d]	0.9 ± 0.03[e]
Heart rate, bpm	712.00 ± 4.06	587.15 ± 50.67[b]	646.00 ± 30.71
FS, %	64.27 ± 0.88	51.01 ± 1.09[a]	62.20 ± 1.38[c]
EF, %	95.40 ± 0.33	88.14 ± 0.78[a]	94.51 ± 0.64[f]

Data are expressed as mean ± standard error of the mean. Vehicle $n=5$; Doxo $n=7$; Doxo+Pargyline $n=5$.

[a]$p<0.001$ *versus* Vehicle, [b]$p<0.01$ *versus* Vehicle, [c]$p<0.001$ *versus* Doxo, [d]$p<0.05$ *versus* Vehicle, [e]$p<0.05$ *versus* Doxo, [f]$p<0.01$ *versus* Doxo.

BW, body weight; EF, ejection fraction.; FS, fractional shortening; IVS, interventricular septum; LVEDD, left ventricular end-diastolic dimension; LVESD, left ventricular end-systolic dimension; LVmass/BW, left ventricular mass normalized to body weight (expressed as mg of left ventricle/gram of body weight mg/g); LVPW, left ventricular posterior wall.

showed increased LV dilation in end-systole (Fig. 7B) and an increase in LV mass normalized to body weight (Fig. 7C and Table 1). In addition, significant decrease in fractional shortening (FS) and ejection fraction (EF), common features of the doxorubicin-induced cardiomyopathy, was clearly evident (Fig. 7D, E and Table 1). Remarkably, LV dilation and function were fully preserved in doxorubicin-treated mice receiving pargyline (Fig. 7 and Table 1). Doxorubicin-treated mice displayed a significant decrease in heart rate, although pargyline treatment did not afford a significant improvement (Fig. 7F).

Discussion

This study shows that MAOs are involved in the oxidative stress induced by doxorubicin treatment in cardiomyocytes. This increase in ROS formation causes mitochondrial dysfunction, which is causally related to all the alterations induced by doxorubicin, including sarcomere disorganization, intracellular [Ca^{2+}] impairment, and eventually cell death. Interestingly, DC is further exacerbated by H_2O_2 or isoproterenol. The causal role of mitochondrial ROS formation and dysfunction is demonstrated by the protective efficacy of MAO inhibition. Remarkably, MAO inhibition proves to be effective also in the *in vivo* model of DC, and completely

prevents LV dilation and cardiac dysfunction in doxorubicin-treated mice.

Our data demonstrate that the treatment with doxorubicin increases H_2O_2 levels only in the mitochondrial compartment. However, the observed elevation in ROS levels is not simply a direct consequence of doxorubicin interaction with Complex I, since MAO inhibition significantly reduced mitochondrial ROS generation. Therefore, MAOs modulate the initial oxidative stress caused by doxorubicin, resulting in a major increase in mitochondrial ROS levels. The beneficial role of MAO inhibition is observed at a doxorubicin concentration (*i.e.*, 0.5 μM) comparable with the one used in clinics. However, it is likely that at higher concentrations, such as those used previously in *in vitro* studies (6, 62), doxorubicin causes a major increase of ROS that is no longer affected by MAO inhibition. The fact that pargyline prevented not only doxorubicin-induced derangements but also those exacerbated by administration of H_2O_2 appears relevant from a pathophysiological and clinical point of view, since a latent DC is likely to be precipitated by comorbidities occurring with doxorubicin (1, 12).

DC is not limited to mitochondria. Indeed, as also reported previously (10, 32, 66), we observed profound alterations in both cardiomyocyte structure and intracellular [Ca^{2+}] homeostasis, which are likely to impair the EC coupling. These changes obviously occur in viable cells. Therefore, DC is accompanied by both cell death and functional changes, which are however both prevented by MAO inhibition.

The absence of an increase in cytosolic ROS levels rules out the possibility that mitochondrial ROS can diffuse to the cytosol, as expected by the abundance of peroxidases and presence of superoxide dismutases (20). Nevertheless, redox communication between mitochondria and cytosol is likely to exist to explain the beneficial effects of pargyline on doxorubicin-induced derangements at the cytosolic level (11, 31). While additional studies are necessary to identify the mechanisms by which mitochondrial oxidative stress is extended to the cytosol, mitochondrial ROS formation appears to be sufficient to explain all the derangements caused by DC. For instance, a recent work highlighted the role of PI3Kγ (38) and also in that case, the triggering factor was suggested to be represented by mitochondrial disruption.

Given the important role played by mitochondrial ROS in DC, various antioxidant treatments have been investigated (*e.g.*, Vitamin A and E, polyunsaturated fatty acids, flavonoids) (9, 43). However, only few of them entered clinical trials, with minor amelioration of cardiac function (9). This failure of antioxidant treatment, which can be extended also to other pathologies (24), can be explained by ROS involvement in both pathological responses and cell defense mechanisms (2, 52). For instance, ischemic preconditioning appears to involve generation of low levels of ROS (20, 56). Indeed, preconditioning protection can be abrogated by antioxidants (29) or replicated by the addition of exogenous oxidants (30). Therefore, the indiscriminate buffer of ROS is potentially able to decrease beneficial responses of tissues (20, 52). In fact, we have recently demonstrated that high levels of selective mitochondrial ROS are deleterious, while low levels of mitochondrial ROS can contribute to cardioprotection in ischemia/reperfusion, both *in vitro* and *in vivo* (2). Thus, a more efficacious approach should identify specific sources of ROS that do not affect other cellular functions. This is especially the case for mitochondria. For instance, if the respiratory complexes were the only sources of ROS, it would not be possible to develop therapeutic approaches since the inhibition of ETC would inevitably impair ATP production and cell viability.

In this respect, MAO inhibition is a valuable tool to demonstrate the involvement of mitochondrial ROS formation in pathophysiology. We have already provided evidence for MAO involvement in cardiac injury induced by postischemic reperfusion, pressure overload, and diabetes, as well as in muscular dystrophy (17, 34, 36, 58). This study further supports and extends this notion, and identifies MAOs as key mediators of doxorubicin-induced cardiotoxicity. This was confirmed in animals injected with doxorubicin, in which concomitant treatment with pargyline prevented LV dilation, increase in LV mass and preserved LV function. Indeed, results from our *in vivo* study strongly suggest that MAO inhibition could prevent cardiac dysfunction and heart failure due to DC also in patients. Nevertheless, our model is more representative of the acute cardiotoxicity that may occur with higher doses of doxorubicin. Future studies will establish if the results obtained from this study apply also to a chronic model of doxorubicin cardiomyopathy.

Growing evidence obtained from animal studies indicates that females might be protected compared with males in relation to DC (42). Interestingly, mitochondrial dysfunction and energy metabolism signaling pathways seem to be associated with early cardiotoxicity in males but not in females (45). In addition, female cardiomyocytes are more resistant to oxidant-induced death (70), while 17-β-estradiol affords cardioprotection in ovariectomized rats treated with doxorubicin (46). In patients, female subjects seem to be more at increased risk of DC, especially when treated with doxorubicin before puberty and adolescence, or after menopause (8). In our *in vivo* study, we used only male mice, and it remains to be established whether MAO inhibition would equally afford protection also in female mice with DC.

Overall, the causal relationship between MAO activity and doxorubicin-induced cardiac derangements suggests that mitochondrial oxidative stress is likely to represent a unifying mechanism of DC. In addition, our data pave the way for the development of MAO inhibitors to prevent cardiac failure in patients treated with doxorubicin.

Limitations of the study

The findings of this study have to be seen in light of some limitations. The first is that the protection elicited by pargyline gives a cytoprotective and cardioprotective role to MAO inhibition, a feature that hardly applies to antitumor interventions. Therefore, it could be hypothesized that MAO inhibition might counteract the antineoplastic efficacy of doxorubicin. This is likely not the case since MAO-A downregulation by shRNA has been shown to protect against tumorigenesis and cancer metastasis (39, 71). In addition, unlike dexrazoxane, MAO inhibitors have no effect on topoisomerase II. Furthermore, they have been used in the clinic for many years, and have never been associated with the development of secondary malignancies. Nevertheless, future studies are necessary to prove that MAO-A and/or

B inhibition, while protecting against DC, does not affect or partially favor the antitumor effect of doxorubicin in cancer patients and across cancer types.

The second limitation is that although our study provides clear evidence of the ability of MAOs to modulate an initial oxidative stress, the underlying mechanism is not yet defined. Additional studies are necessary to clarify whether doxorubicin affects directly the structural–functional relationship of MAO or its interaction with the lipid components of the outer mitochondrial membrane. In addition, besides H_2O_2 formation, MAOs are a source of reactive aldehydes and ammonia (35). Since DC is also associated with changes in cytotoxic aldehydes, and mitochondrial aldehyde dehydrogenase (ALDH2) ameliorates DC (63), it is plausible that MAO inhibition in DC abolishes the detrimental effects of these reactive aldehydes as well. Additional studies are necessary to quantitate the relative contribution to DC given by ROS and aldehydes produced by MAOs.

Materials and Methods

Animals and procedures

All animal studies were performed using male C57BL6/J mice at 12 weeks of age. Animals were injected intraperitoneally with 10 mg/kg doxorubicin (Sigma) using saline solution as vehicle. The same day of the doxorubicin injection, mice were randomized and subjected to a daily treatment with either vehicle or MAO inhibitor pargyline (50 mg/kg/day, i.p.; Sigma). Animals were observed and weighed daily for 5 weeks, and were sacrificed when they exhibited distress and/or when weight loss approached 25%.

Experiments were carried out in the animal facility of the Department of Experimental Oncology of the European Institute of Oncology (Ministry of Health authorization: DM No. 86/2005-17/06/2005). All aspects of animal care and experimentation were performed in accordance with the Guide for the Care and Use of Laboratory Animals published by the US National Institutes of Health (NIH Publication No. 85-23, revised 1996) and the Italian Laws (D.L.vo 116/92 and after additions), which enforces EU86/609 Directive. Experiments were approved by the local Ethical Committee and notified to the Ministry of Health (Project No. 13/2010).

Echocardiography

In vivo cardiac morphology and function were assessed by serial M-mode echocardiography (Acuson Sequoia C256, 13 MHz transducer; Siemens, PA) performed in conscious mice. LV end-systolic and end-diastolic dimensions were averaged from three to five beats. LV percent FS, EF, and LV mass were calculated as described previously (36). Thickness of posterior free wall and interventricular septum was averaged.

Cell culture and treatments

NRVMs were isolated from 1- to 3-day-old Wistar rats as previously described (34). Cardiomyocytes were plated in 0.1% porcine gelatin (Sigma)-coated plates at variable densities ($\sim 2.5 \times 10^5$ cells/mL) in MEM supplemented with 10% fetal bovine serum (FBS; Thermo Fisher Scientific), 1% penicillin/streptomycin (Thermo Fisher Scientific), 1% nonessential amino acids (Thermo Fisher Scientific), 1 m*M* 5-bromo-2-deoxyuridine (Sigma). Cells were maintained at 37°C in the presence of 5% CO_2. The medium was changed to MEM supplemented with 1% FBS, 1% penicillin/streptomycin, and 1% nonessential amino acids after 24 h of plating.

AMVMs were isolated from the hearts of 12-week-old C57Bl6/J mice, as previously described (36). Collagenase-digested isolated myocytes were incubated in buffer with increasing concentrations of Ca^{2+}, achieving a final concentration of 1.2 m*M* Ca^{2+} as in Dulbecco's modified Eagle's medium (DMEM) plating media. Cells were seeded at 6×10^4 rod-shaped myocytes per milliliter in DMEM plating media supplemented with 10 m*M* 2,3-butanedione monoxime (Sigma) in plates coated with laminin. Cells were maintained at 37°C in the presence of 5% CO_2. The medium was replaced after 1 h incubation to remove unattached cells.

To evaluate the effect of doxorubicin, cells were pretreated with 0.5 μM doxorubicin (32, 44), in the presence or the absence of 100 μM pargyline (Sigma), unless differently specified in the results. To induce oxidative stress, cells were treated with different concentrations of exogenous H_2O_2, ranging from 1 to 100 μM. To stimulate MAO-A in intact NRVMs, cells were treated with 20 μM tyramine for 2 h (36).

Live imaging

Experiments were carried out in HBSS at pH 7.4 (adjusted with NaOH) and at 37°C. Images were acquired using an inverted fluorescence microscope (Leica DMI6000B equipped with DFC365FX camera) with PL APO 40×/1.25 oil objective. Fluorescence intensity was quantified using the Fiji distribution of the Java-based image processing program ImageJ (55), and background signal was subtracted from all analyzed regions of interest. For Ca^{2+} imaging, traces were analyzed using the ''Peak Analyzer'' tool of Origin Pro 9.1.

To silence MAO-A expression, NRVMs were transfected with scramble or MAO-A siRNA (Ambion) as previously described (18). The efficiency of MAO-A knockdown was assessed by Western blotting (Supplementary Fig. S1B).

To monitor mitochondrial and cytosolic ROS formation in NRVMs, cells were transfected with the genetically encoded H_2O_2 sensors Mito-HyPer and Cyto-HyPer (Evrogen) (4). To monitor mitochondrial GSSG/GSH ratio in NRVMs, cells were transfected with the genetically encoded sensor Mito-Grx1-roGFP. pLPCX mito Grx1-roGFP2 was a gift from Tobias Dick (Addgene Plasmid No. 64977; RRID: Addgene_64977) (28). NRVMs were plated on μ-Plate 96-well black plates (Ibidi) at a density of 4×10^4 cells/well, and transfected with Lipofectamine 3000 reagent (Sigma). For each transfection, 0.1 μg of plasmid was diluted in 5 μL of Opti-MEM medium (Thermo Fisher Scientific) in the presence of 0.2 μL of P3000™ reagent (Life Technologies), and later combined with 0.3 μL of Lipofectamine™ 3000 (Life Technologies). The DNA–lipid complexes were added to the cells and incubated at 37°C in the presence of 5% CO_2. Transfected cells were used for experiments after 48 h. Fluorescence values were expressed as HyPer ratio (488/410 nm) and Grx1-roGFP ratio (410/488).

To monitor mitochondrial ROS in AMVMs, cells were incubated with 250 n*M* MTR CM-H_2XRos (Thermo Fisher Scientific) for 30 min at 37°C, in the presence of 5% CO_2. Since the accumulation of MTR in cells can vary from different preparations, data were normalized to the dimethyl sulfoxide (DMSO) control.

To monitor $\Delta\Psi m$, cells were incubated with 25 n*M* TMRM (Thermo Fisher Scientific) and 1.6 μM cyclosporin H for 30 min at 37°C, in the presence of 5% CO_2. TMRM fluorescence intensity was monitored, and images were acquired before and after the addition of 4 μM carbonyl cyanide-*p*-trifluoromethoxyphenylhydrazone (FCCP; Sigma) (34). To obtain a reliable value for TMRM, fluorescence values were expressed as ΔF (F_0/F_{FCCP}), and results were normalized to the DMSO control basal value.

To monitor PTP opening, cells were incubated with 1 μM calcein acetoxymethyl (AM) ester (Thermo Fisher Scientific) in the presence of 2 m*M* cobalt chloride for 15 min at 37°C in a humidified incubator, followed by 20 min of de-esterification as previously described (50). PTP opening was induced by 5 μM of the Ca^{2+} ionophore calcimycin. To evaluate the extent of pore opening, data were normalized to the basal value.

To monitor intracellular [Ca^{2+}] homeostasis, cells were incubated with 5 μM Fluo-4 AM ester (Thermo Fisher Scientific), 0.01% w/v pluronic F-127 (Sigma), and 250 μM sulfinpyrazone (Sigma), for 20 min at 37°C in a humidified incubator, followed by 20 min of de-esterification. Caffeine stimulus was applied to NRVMs in the presence or absence of 10 μM isoproterenol (Sigma) (74). Since the accumulation of Fluo-4 in NRVMs can vary from different preparations, data were normalized to the DMSO control. The fractional release of Ca^{2+} was evaluated to define the fraction of SR Ca^{2+} released at every twitch (3).

Glutathione redox state estimation in cell lysates

NRVMs were plated in six-well plates at a density of 5×10^5 cells/well. At day 4, cells were treated with 0.5 μM doxorubicin for 24 h, in the presence or the absence of 100 μM pargyline. The day after, NRVMs were collected, washed twice with cold phosphate-buffered saline (PBS), and then lysed and deproteinized with 6% *meta*-phosphoric acid. After 10 min at 4°C, samples were centrifuged, and supernatants were neutralized with 15% Na_3PO_4 and assayed for total glutathione as previously described (68). Samples were derivatized with 2-vinylpyridine to block reduced glutathione, and oxidized glutathione was then estimated. Total glutathione was normalized to protein level, and data expressed as the percentage of oxidized glutathione (GSSG) normalized to total glutathione (GSH tot).

Total thiol estimation

NRVMs well plated in six-well plates at a density of 5×10^5 cells/well. At day 4, cells were treated with 0.5 μM doxorubicin for 24 h, in the presence or the absence of 100 μM pargyline. After the treatment, cells were washed with 1 mL of PBS 1 × and then dissolved with 1 mL of 0.2 *M* Tris/HCl (pH 8.1), 5 m*M* EDTA, and 7.2 *M* guanidine. The reaction was started by the addition of 0.1 *M* DTNB [5,5′-dithiobis(2-nitrobenzoic acid)]. The absorbance of the DTNB reduction product was followed at 412 nm at 25°C (68).

Lipid peroxidation assay

Lipid peroxidation was estimated as previously described (67). NRVMs were plated in six-well plates at a density of 5×10^5 cells/well. At day 4, cells were treated with 0.5 μM doxorubicin for 24 h, in the presence or the absence of 100 μM pargyline. Cells were washed with 1 mL of PBS 1 ×. Subsequently, cells were disrupted with 1 mL of 0.1 N sulfuric acid and 0.15 mL of 10% phosphotungstic acid (PTA), and incubated for 10 min at room temperature. Then, samples were centrifuged at 11,600 *g* for 10 min. The supernatant was removed, and 1 mL of 0.1 N H_2SO_4 and 0.15 mL of 10% PTA were added to the pellets. After 5 min of incubation at room temperature, samples were centrifuged as described above. The supernatant was removed, and the dried pellet was dissolved in 0.35% NONIDET, 0.014% butylated hydroxytoluene (BHT), and 0.23% thiobarbituric acid in a final volume of 0.25 mL. Subsequently, samples were incubated at 95°C for 60 min. After this time, samples were cooled on ice for 5 min and centrifuged at 11,600 *g* for 10 min. The pellets were discarded, and 0.4 mL of *n*-butanol were added to the supernatants, vigorously mixed, and centrifuged at 11,600 *g* for 15 min. MDA is present in the upper phase. The fluorescence of the latter was analyzed at 530 nm (Ex) and at 590 nm (Em) using a Tecan plate reader. Incubation with 25 m*M* cumene hydroperoxide and 50 μM hemin for 15 min, or with 100 μM H_2O_2 for 1 h was used as the positive control (Supplementary Fig. S3A). Data are expressed as fluorescence per milligram proteins normalized *versus* control.

Western blot analysis

NRVMs were plated in 6-well plates at a density of 4×10^5 cells/mL, while AMVMs were plated in 12-well plates at a density of 6×10^4 rod-shaped myocytes per milliliter. Cells were incubated for 24 h with 0.5 μM doxorubicin, in the presence or absence of 100 μM pargyline. For the assessment of autophagy flux, cells were treated with 20 m*M* ammonium chloride and 100 μM leupeptin 4 h before cell lysis. Cells were homogenized in RIPA Lysis Buffer (1 ×; EMD Millipore) containing protease (1 ×, cOmplete mini protease inhibitor cocktail; Roche) and phosphatase (1 ×, PhosStop; Roche) inhibitors. Protein concentration was determined using BCA protein assay (BCA Kit; Euroclone). Proteins were separated using 4%–12% Bis-Tris gels (Life Technologies) in 2-(N-Morpholino) ethanesulfonic acid (MES)/SDS (sodium dodecyl sulfate) running buffer 1 × (*i.e.*, 1 *M* MES, 1 *M* Tris Base, 69.3 m*M* SDS, 20.5 m*M* EDTA, pH 7.3). Proteins were transferred to nitrocellulose membrane (Bio-Rad) by Western blotting in transfer buffer (*i.e.*, 250 m*M* Tris Base, 1.92 *M* glycine, 0.1% SDS) overnight at 4°C. Membranes were blocked for 1 h with 3% bovine serum albumin (BSA) in TBS-Tween, and incubated overnight with the following primary antibodies diluted in 3% BSA:

Anti-MAO-A → 1:1000 (ab126751, Rabbit; Abcam)
Anti-MAO-B → 1:1000 (M1821, Rabbit; Sigma)
Anti-LC3B → 1:1000 (#2775, Rabbit; Cell Signaling)
Anti-p62 → 1:1000 (P0067, Rabbit; Sigma)
Antiactin →1:1000 (sc-56459, Mouse; Santa Cruz Biotechnology)

After incubation with primary antibodies, membranes were washed three times in TBS-Tween, 5 min each, and incubated for 1 h with the following secondary antibodies diluted in 3% BSA:

Antimouse (m-IgGκ BP-HRP) →1:3000 (#sc-516102; Santa Cruz Biotechnology)
Antirabbit (mouse antirabbit IgG-HRP) →1:3000 (#sc-2357; Santa Cruz Biotechnology)

After incubation with primary and secondary HRP-conjugated antibodies, bands were detected by the Pierce™ ECL Western Blotting Substrate using the UVITEC Cambridge, mini-HD instrument. Bands were quantified by densitometry analysis performed using the Fiji distribution of the Java-based image processing program ImageJ (55).

Immunocytochemistry

NRVMs were plated in 24-well plates on gelatin-coated coverslips at a density of 5×10^4 cells/well. At day 4, cells were treated with 0.5 μM doxorubicin for 24 h, in the presence or absence of 100 μM pargyline. The day after, NRVMs were treated with 10 μM H_2O_2 for 1 h. NRVMs were fixed with 4% paraformaldehyde in PBS for 30 min at room temperature, permeabilized with PBS supplemented with 1% saponin for 15 min, and blocked with 3% BSA for 1 h at 4°C. After blocking, mitochondria were stained using rabbit anti-TOM20 antibody (1:500; Santa Cruz Biotechnology), while sarcomeres were stained using mouse anti-α-sarcomeric actinin antibody (1:500; Life Technologies) overnight at 4°C. The day after, samples were incubated with Alexa Fluor 594-conjugated antirabbit (1:250; Life Technologies) and Alexa Fluor 488-conjugated antimouse (1:250; Life Technologies) secondary antibodies for 1 h at room temperature. Coverslips were mounted using ProLong Diamond Antifade Mountant with DAPI to stain nuclei (Life Technologies). Images were collected at Zeiss LSM 700 confocal system equipped with a PlanApo 40×/1.2 oil objective, and an Argon laser was used to excite the fluorophores at the appropriate wavelength. Images were collected at 2048×2048 pixels per image with a 100 Hz acquisition rate. Images were analyzed using the Fiji distribution of the Java-based image processing program ImageJ (55).

Analysis of mitochondrial subcellular distribution

The evaluation of mitochondrial subcellular distribution was obtained based on the method described by Spinazzi *et al.* (59). In brief, mitochondria were stained using rabbit anti-TOM20 antibody, sarcomeres were stained using mouse anti-α-sarcomeric actinin, and images were collected and analyzed as described in the Immunocytochemistry Section. For each cell, a region of interest (ROI) was drawn based on the contours identified by the α-sarcomeric staining. For a given ROI, we computed a distribution parameter R defined as $R=F/F_{max}$, where F is TOM20 mean fluorescence of the ROI, and F_{max} is the highest fluorescence value. The R parameter was comprised between 0 and 1, and it was expected to have higher values in cells with homogeneous mitochondrial distribution (*i.e.*, F will be closer to F_{max}) compared with cells displaying alterations in mitochondrial distribution.

Transmission electron microscopy

TEM imaging of cells was performed as described before (26). In brief, cells were plated at a density of 10^5 cells/well in a 24-well plate, and they were treated with 0.5 μM doxorubicin for 24 h in the presence or absence of 100 μM pargyline. The day after, NRVMs were treated with 10 μM H_2O_2 for 1 h. Cells were fixed for 1 h at 37°C with freshly prepared 1.25% (v/v) glutaraldehyde in 0.1 M sodium cacodylate, pH 7.4. After washing with 0.1 M sodium cacodylate, cells were postfixed in 1% OsO_4, 1.5% $K_4Fe(CN)_6$ in 0.1 M sodium cacodylate, pH 7.4, stained with 0.5% uranyl acetate, dehydrated in ethanol, and embedded in Embed 812. Sample sections were imaged on a Tecnai G2 (FEI) transmission electron microscope operating at 100 kV at the EM Facility of the University of Padova. Images were captured using a Veleta (Olimpus Imaging System) digital camera (pixel size 13×13 μm; pixel size at a 46,000× magnification with screen magnification of $3\times0.1\times0.1$ nm). Mitochondrial perimeter was quantified using the ROI Manager plug-in of the Fiji distribution of the Java-based image processing program ImageJ (55).

Assessment of cell death

To monitor apoptosis, NRVMs were seeded in μ-Slide eight-well plates (Ibidi) at a density of 4×10^4 cells/well, and incubated with 0.5 μM doxorubicin for 24 h in the presence or absence of 100 μM pargyline. The day after, cells were incubated with Annexin-V-Fluos (1:200; Sigma) following manufacturer's instructions for 15 min at room temperature in the dark (13). Positive cells have been evaluated in relation to the total number of cells identified in bright field in every field of view analyzed. Incubation with 2 μM Staurosporine for 1 h was used as positive control (Supplementary Fig. S3C). Data are expressed as percentage of the total cell number.

The release of LDH from NRVMs was measured to evaluate cell death as described before (19). NRVMs were seeded in 24-well plates at a density of 1.5×10^5 cells/well, and incubated with 0.5 μM doxorubicin for 24 h in the presence or absence of 100 μM pargyline. The day after, medium was replaced with HBSS at pH 7.4 (adjusted with NaOH), and cells were incubated with different concentrations of H_2O_2 (*i.e.*, 10–100 μM H_2O_2). Supernatant aliquots were collected at different time points after the incubation with H_2O_2 (*i.e.*, 1–3–6 h). At the end of every experiment, intact cells were lysed by incubating with 1% Triton X-100 (Sigma) for 30 min, and supernatants were collected to evaluate the total amount of LDH. LDH enzymatic activity was measured spectrophotometrically by the absorbance of nicotinamide adenine dinucleotide (Roche) at 340 nm, indicative of the reduction of pyruvate to lactate.

Data analysis

All values are expressed as mean ± standard error of the mean. Comparison between groups was performed by one-way ANOVA, followed by Tukey's *post hoc* multiple comparison where data were normally distributed. Data that did not follow the normal distribution were statistically analyzed by Kruskal–Wallis ANOVA. Comparisons between two groups were performed using two-tailed Student's t-test. A value of $p<0.05$ was considered significant.

Acknowledgments

We thank Dr. Djahida Bedja for expert technical assistance and Dr. Federico Caicci (EM Facility, Department of Biology, University of Padova) for the TEM analysis.

Author Disclosure Statement

No competing financial interests exist.

Funding Information

This work was supported by the Leducq Transatlantic Network of Excellence 16CVD04 (F.D.L.) and the COST Action EU-CARDIOPROTECTION CA16225 (F.D.L.); S.A., M.D.S., and N.K. are Fellows of the Leducq Transatlantic Network of Excellence.

Supplementary Material

Supplementary Figure S1
Supplementary Figure S2
Supplementary Figure S3

References

1. Ali MK, Ewer MS, Gibbs HR, Swafford J, and Graff KL. Late doxorubicin-associated cardiotoxicity in children. The possible role of intercurrent viral infection. *Cancer* 74: 182–188, 1994.
2. Antonucci S, Mulvey JF, Burger N, Di Sante M, Hall AR, Hinchy EC, Caldwell ST, Gruszczyk AV, Deshwal S, Hartley RC, Kaludercic N, Murphy MP, Di Lisa F, and Krieg T. Selective mitochondrial superoxide generation in vivo is cardioprotective through hormesis. *Free Radic Biol Med* 134: 678–687, 2019.
3. Bassani JW, Bassani RA, and Bers DM. Twitch-dependent SR Ca accumulation and release in rabbit ventricular myocytes. *Am J Physiol* 265: C533–C540, 1993.
4. Belousov VV, Fradkov AF, Lukyanov KA, Staroverov DB, Shakhbazov KS, Terskikh AV, and Lukyanov S. Genetically encoded fluorescent indicator for intracellular hydrogen peroxide. *Nat Methods* 3: 281–286, 2006.
5. Benard G, Bellance N, James D, Parrone P, Fernandez H, Letellier T, and Rossignol R. Mitochondrial bioenergetics and structural network organization. *J Cell Sci* 120: 838–848, 2007.
6. Berthiaume JM and Wallace KB. Adriamycin-induced oxidative mitochondrial cardiotoxicity. *Cell Biol Toxicol* 23: 15–25, 2007.
7. Binda C, Newton-Vinson P, Hubalek F, Edmondson DE, and Mattevi A. Structure of human monoamine oxidase B, a drug target for the treatment of neurological disorders. *Nat Struct Biol* 9: 22–26, 2002.
8. Cadeddu Dessalvi C, Pepe A, Penna C, Gimelli A, Madonna R, Mele D, Monte I, Novo G, Nugara C, Zito C, Moslehi JJ, de Boer RA, Lyon AR, Tocchetti CG, and Mercuro G. Sex differences in anthracycline-induced cardiotoxicity: the benefits of estrogens. *Heart Fail Rev* 24: 915–925, 2019.
9. Cappetta D, De Angelis A, Sapio L, Prezioso L, Illiano M, Quaini F, Rossi F, Berrino L, Naviglio S, and Urbanek K. Oxidative stress and cellular response to doxorubicin: a common factor in the complex milieu of anthracycline cardiotoxicity. *Oxid Med Cell Longev* 2017: 1521020, 2017.
10. Cardinale D, Colombo A, Lamantia G, Colombo N, Civelli M, De Giacomi G, Rubino M, Veglia F, Fiorentini C, and Cipolla CM. Anthracycline-induced cardiomyopathy: clinical relevance and response to pharmacologic therapy. *J Am Coll Cardiol* 55: 213–220, 2010.
11. Chandel NS. Mitochondria as signaling organelles. *BMC Biol* 12: 34, 2014.
12. Chen MH, Colan SD, and Diller L. Cardiovascular disease: cause of morbidity and mortality in adult survivors of childhood cancers. *Circ Res* 108: 619–628, 2011.
13. Ciscato F, Filadi R, Masgras I, Pizzi M, Marin O, Damiano N, Pizzo P, Gori A, Frezzato F, Chiara F, Trentin L, Bernardi P, and Rasola A. Hexokinase 2 displacement from mitochondria-associated membranes prompts Ca(2+) -dependent death of cancer cells. *EMBO Rep* e49117, 2020. [Epub ahead of print]; DOI: 10.15252/embr.201949117.
14. Ciscato F, Sciacovelli M, Villano G, Turato C, Bernardi P, Rasola A, and Pontisso P. SERPINB3 protects from oxidative damage by chemotherapeutics through inhibition of mitochondrial respiratory complex I. *Oncotarget* 5: 2418–2427, 2014.
15. Deng S, Kruger A, Kleschyov AL, Kalinowski L, Daiber A, and Wojnowski L. Gp91phox-containing NAD(P)H oxidase increases superoxide formation by doxorubicin and NADPH. *Free Radic Biol Med* 42: 466–473, 2007.
16. Deshwal S, Antonucci S, Kaludercic N, and Di Lisa F. Measurement of mitochondrial ROS formation. *Methods Mol Biol* 1782: 403–418, 2018.
17. Deshwal S, Di Sante M, Di Lisa F, and Kaludercic N. Emerging role of monoamine oxidase as a therapeutic target for cardiovascular disease. *Curr Opin Pharmacol* 33: 64–69, 2017.
18. Deshwal S, Forkink M, Hu CH, Buonincontri G, Antonucci S, Di Sante M, Murphy MP, Paolocci N, Mochly-Rosen D, Krieg T, Di Lisa F, and Kaludercic N. Monoamine oxidase-dependent endoplasmic reticulum-mitochondria dysfunction and mast cell degranulation lead to adverse cardiac remodeling in diabetes. *Cell Death Differ* 25: 1671–1685, 2018.
19. Di Lisa F, Menabo R, Canton M, Barile M, and Bernardi P. Opening of the mitochondrial permeability transition pore causes depletion of mitochondrial and cytosolic NAD+ and is a causative event in the death of myocytes in postischemic reperfusion of the heart. *J Biol Chem* 276: 2571–2575, 2001.
20. Egea J, Fabregat I, Frapart YM, Ghezzi P, Gorlach A, Kietzmann T, Kubaichuk K, Knaus UG, Lopez MG, Olaso-Gonzalez G, Petry A, Schulz R, Vina J, Winyard P, Abbas K, Ademowo OS, Afonso CB, Andreadou I, Antelmann H, Antunes F, Aslan M, Bachschmid MM, Barbosa RM, Belousov V, Berndt C, Bernlohr D, Bertran E, Bindoli A, Bottari SP, Brito PM, Carrara G, Casas AI, Chatzi A, Chondrogianni N, Conrad M, Cooke MS, Costa JG, Cuadrado A, My-Chan Dang P, De Smet B, Debelec-Butuner B, Dias IHK, Dunn JD, Edson AJ, El Assar M, El-Benna J, Ferdinandy P, Fernandes AS, Fladmark KE, Forstermann U, Giniatullin R, Giricz Z, Gorbe A, Griffiths H, Hampl V, Hanf A, Herget J, Hernansanz-Agustin P, Hillion M, Huang J, Ilikay S, Jansen-Durr P, Jaquet V, Joles JA, Kalyanaraman B, Kaminskyy D, Karbaschi M, Kleanthous M, Klotz LO, Korac B, Korkmaz KS, Koziel R, Kracun D, Krause KH, Kren V, Krieg T, Laranjinha J, Lazou A, Li H, Martinez-Ruiz A, Matsui R, McBean GJ, Meredith SP, Messens J, Miguel V, Mikhed Y, Milisav I, Milkovic L, Miranda-Vizuete A, Mojovic M, Monsalve M, Mouthuy PA, Mulvey J, Munzel T, Muzykantov V, Nguyen ITN, Oelze M, Oliveira NG, Palmeira CM, Papaevgeniou N, Pavicevic A, Pedre B, Peyrot F, Phylactides M, Pircalabioru GG, Pitt AR, Poulsen HE, Prieto I, Rigobello MP,

Robledinos-Anton N, Rodriguez-Manas L, Rolo AP, Rousset F, Ruskovska T, Saraiva N, Sasson S, Schroder K, Semen K, Seredenina T, Shakirzyanova A, Smith GL, Soldati T, Sousa BC, Spickett CM, Stancic A, Stasia MJ, Steinbrenner H, Stepanic V, Steven S, Tokatlidis K, Tuncay E, Turan B, Ursini F, Vacek J, Vajnerova O, Valentova K, Van Breusegem F, Varisli L, Veal EA, Yalcin AS, Yelisyeyeva O, Zarkovic N, Zatloukalova M, Zielonka J, Touyz RM, Papapetropoulos A, Grune T, Lamas S, Schmidt H, Di Lisa F, and Daiber A. European contribution to the study of ROS: a summary of the findings and prospects for the future from the COST action BM1203 (EU-ROS). *Redox Biol* 13: 94–162, 2017.

21. Eschenhagen T, Force T, Ewer MS, de Keulenaer GW, Suter TM, Anker SD, Avkiran M, de Azambuja E, Balligand JL, Brutsaert DL, Condorelli G, Hansen A, Heymans S, Hill JA, Hirsch E, Hilfiker-Kleiner D, Janssens S, de Jong S, Neubauer G, Pieske B, Ponikowski P, Pirmohamed M, Rauchhaus M, Sawyer D, Sugden PH, Wojta J, Zannad F, and Shah AM. Cardiovascular side effects of cancer therapies: a position statement from the Heart Failure Association of the European Society of Cardiology. *Eur J Heart Fail* 13: 1–10, 2011.
22. Fajardo G, Zhao M, Powers J, and Bernstein D. Differential cardiotoxic/cardioprotective effects of beta-adrenergic receptor subtypes in myocytes and fibroblasts in doxorubicin cardiomyopathy. *J Mol Cell Cardiol* 40: 375–383, 2006.
23. Ferrans VJ, Clark JR, Zhang J, Yu ZX, and Herman EH. Pathogenesis and prevention of doxorubicin cardiomyopathy. *Tsitologiia* 39: 928–937, 1997.
24. Fortmann SP, Burda BU, Senger CA, Lin JS, and Whitlock EP. Vitamin and mineral supplements in the primary prevention of cardiovascular disease and cancer: an updated systematic evidence review for the U.S. Preventive Services Task Force. *Ann Intern Med* 159: 824–834, 2013.
25. Geisberg CA and Sawyer DB. Mechanisms of anthracycline cardiotoxicity and strategies to decrease cardiac damage. *Curr Hypertens Rep* 12: 404–410, 2010.
26. Glytsou C, Calvo E, Cogliati S, Mehrotra A, Anastasia I, Rigoni G, Raimondi A, Shintani N, Loureiro M, Vazquez J, Pellegrini L, Enriquez JA, Scorrano L, and Soriano ME. Optic atrophy 1 is epistatic to the core MICOS component MIC60 in mitochondrial cristae shape control. *Cell Rep* 17: 3024–3034, 2016.
27. Gordon RR, Wu M, Huang CY, Harris WP, Sim HG, Lucas JM, Coleman I, Higano CS, Gulati R, True LD, Vessella R, Lange PH, Garzotto M, Beer TM, and Nelson PS. Chemotherapy-induced monoamine oxidase expression in prostate carcinoma functions as a cytoprotective resistance enzyme and associates with clinical outcomes. *PLoS One* 9: e104271, 2014.
28. Gutscher M, Pauleau AL, Marty L, Brach T, Wabnitz GH, Samstag Y, Meyer AJ, and Dick TP. Real-time imaging of the intracellular glutathione redox potential. *Nat Methods* 5: 553–559, 2008.
29. Hao J, Li WW, Du H, Zhao ZF, Liu F, Lu JC, Yang XC, and Cui W. Role of vitamin C in cardioprotection of ischemia/reperfusion injury by activation of mitochondrial KATP channel. *Chem Pharm Bull (Tokyo)* 64: 548–557, 2016.
30. Hegstad AC, Antonsen OH, and Ytrehus K. Low concentrations of hydrogen peroxide improve post-ischaemic metabolic and functional recovery in isolated perfused rat hearts. *J Mol Cell Cardiol* 29: 2779–2787, 1997.
31. Hinchy EC, Gruszczyk AV, Willows R, Navaratnam N, Hall AR, Bates G, Bright TP, Krieg T, Carling D, and Murphy MP. Mitochondria-derived ROS activate AMP-activated protein kinase (AMPK) indirectly. *J Biol Chem* 293: 17208–17217, 2018.
32. Ikeda S, Matsushima S, Okabe K, Ikeda M, Ishikita A, Tadokoro T, Enzan N, Yamamoto T, Sada M, Deguchi H, Morimoto S, Ide T, and Tsutsui H. Blockade of L-type Ca(2+) channel attenuates doxorubicin-induced cardiomyopathy via suppression of CaMKII-NF-kappaB pathway. *Sci Rep* 9: 9850, 2019.
33. Jain D. Cardiotoxicity of doxorubicin and other anthracycline derivatives. *J Nucl Cardiol* 7: 53–62, 2000.
34. Kaludercic N, Carpi A, Nagayama T, Sivakumaran V, Zhu G, Lai EW, Bedja D, De Mario A, Chen K, Gabrielson KL, Lindsey ML, Pacak K, Takimoto E, Shih JC, Kass DA, Di Lisa F, and Paolocci N. Monoamine oxidase B prompts mitochondrial and cardiac dysfunction in pressure overloaded hearts. *Antioxid Redox Signal* 20: 267–280, 2014.
35. Kaludercic N, Mialet-Perez J, Paolocci N, Parini A, and Di Lisa F. Monoamine oxidases as sources of oxidants in the heart. *J Mol Cell Cardiol* 73: 34–42, 2014.
36. Kaludercic N, Takimoto E, Nagayama T, Feng N, Lai EW, Bedja D, Chen K, Gabrielson KL, Blakely RD, Shih JC, Pacak K, Kass DA, Di Lisa F, and Paolocci N. Monoamine oxidase A-mediated enhanced catabolism of norepinephrine contributes to adverse remodeling and pump failure in hearts with pressure overload. *Circ Res* 106: 193–202, 2010.
37. Kokoszka JE, Coskun P, Esposito LA, and Wallace DC. Increased mitochondrial oxidative stress in the Sod2 (+/-) mouse results in the age-related decline of mitochondrial function culminating in increased apoptosis. *Proc Natl Acad Sci U S A* 98: 2278–2283, 2001.
38. Li M, Sala V, De Santis MC, Cimino J, Cappello P, Pianca N, Di Bona A, Margaria JP, Martini M, Lazzarini E, Pirozzi F, Rossi L, Franco I, Bornbaum J, Heger J, Rohrbach S, Perino A, Tocchetti CG, Lima BHF, Teixeira MM, Porporato PE, Schulz R, Angelini A, Sandri M, Ameri P, Sciarretta S, Lima-Junior RCP, Mongillo M, Zaglia T, Morello F, Novelli F, Hirsch E, and Ghigo A. Phosphoinositide 3-kinase gamma inhibition protects from anthracycline cardiotoxicity and reduces tumor growth. *Circulation* 138: 696–711, 2018.
39. Li PC, Siddiqi IN, Mottok A, Loo EY, Wu CH, Cozen W, Steidl C, and Shih JC. Monoamine oxidase A is highly expressed in classical Hodgkin lymphoma. *J Pathol* 243: 220–229, 2017.
40. Lim CC, Zuppinger C, Guo X, Kuster GM, Helmes M, Eppenberger HM, Suter TM, Liao R, and Sawyer DB. Anthracyclines induce calpain-dependent titin proteolysis and necrosis in cardiomyocytes. *J Biol Chem* 279: 8290–8299, 2004.
41. Lipshultz SE, Scully RE, Lipsitz SR, Sallan SE, Silverman LB, Miller TL, Barry EV, Asselin BL, Athale U, Clavell LA, Larsen E, Moghrabi A, Samson Y, Michon B, Schorin MA, Cohen HJ, Neuberg DS, Orav EJ, and Colan SD. Assessment of dexrazoxane as a cardioprotectant in doxorubicin-treated children with high-risk acute lymphoblastic leukaemia: long-term follow-up of a prospective, randomised, multicentre trial. *Lancet Oncol* 11: 950–961, 2010.
42. Meiners B, Shenoy C, and Zordoky BN. Clinical and preclinical evidence of sex-related differences in anthracycline-induced cardiotoxicity. *Biol Sex Differ* 9: 38, 2018.

43. Milei J, Boveris A, Llesuy S, Molina HA, Storino R, Ortega D, and Milei SE. Amelioration of adriamycin-induced cardiotoxicity in rabbits by prenylamine and vitamins A and E. *Am Heart J* 111: 95–102, 1986.
44. Minotti G, Menna P, Salvatorelli E, Cairo G, and Gianni L. Anthracyclines: molecular advances and pharmacologic developments in antitumor activity and cardiotoxicity. *Pharmacol Rev* 56: 185–229, 2004.
45. Moulin M, Piquereau J, Mateo P, Fortin D, Rucker-Martin C, Gressette M, Lefebvre F, Gresikova M, Solgadi A, Veksler V, Garnier A, and Ventura-Clapier R. Sexual dimorphism of doxorubicin-mediated cardiotoxicity: potential role of energy metabolism remodeling. *Circ Heart Fail* 8: 98–108, 2015.
46. Munoz-Castaneda JR, Montilla P, Munoz MC, Bujalance I, Muntane J, and Tunez I. Effect of 17-beta-estradiol administration during adriamycin-induced cardiomyopathy in ovariectomized rat. *Eur J Pharmacol* 523: 86–92, 2005.
47. Murphy MP. How mitochondria produce reactive oxygen species. *Biochem J* 417: 1–13, 2009.
48. Octavia Y, Tocchetti CG, Gabrielson KL, Janssens S, Crijns HJ, and Moens AL. Doxorubicin-induced cardiomyopathy: from molecular mechanisms to therapeutic strategies. *J Mol Cell Cardiol* 52: 1213–1225, 2012.
49. Pal S, Ahir M, and Sil PC. Doxorubicin-induced neurotoxicity is attenuated by a 43-kD protein from the leaves of *Cajanus indicus* L. via NF-kappaB and mitochondria dependent pathways. *Free Radic Res* 46: 785–798, 2012.
50. Petronilli V, Miotto G, Canton M, Brini M, Colonna R, Bernardi P, and Di Lisa F. Transient and long-lasting openings of the mitochondrial permeability transition pore can be monitored directly in intact cells by changes in mitochondrial calcein fluorescence. *Biophys J* 76: 725–734, 1999.
51. Riccio G, Antonucci S, Coppola C, D'Avino C, Piscopo G, Fiore D, Maurea C, Russo M, Rea D, Arra C, Condorelli G, Di Lisa F, Tocchetti CG, De Lorenzo C, and Maurea N. Ranolazine attenuates trastuzumab-induced heart dysfunction by modulating ROS production. *Front Physiol* 9: 38, 2018.
52. Ristow M. Unraveling the truth about antioxidants: mitohormesis explains ROS-induced health benefits. *Nat Med* 20: 709–711, 2014.
53. Sag CM, Kohler AC, Anderson ME, Backs J, and Maier LS. CaMKII-dependent SR Ca leak contributes to doxorubicin-induced impaired Ca handling in isolated cardiac myocytes. *J Mol Cell Cardiol* 51: 749–759, 2011.
54. Salvatorelli E, Guarnieri S, Menna P, Liberi G, Calafiore AM, Mariggio MA, Mordente A, Gianni L, and Minotti G. Defective one- or two-electron reduction of the anticancer anthracycline epirubicin in human heart. Relative importance of vesicular sequestration and impaired efficiency of electron addition. *J Biol Chem* 281: 10990–11001, 2006.
55. Schindelin J, Arganda-Carreras I, Frise E, Kaynig V, Longair M, Pietzsch T, Preibisch S, Rueden C, Saalfeld S, Schmid B, Tinevez JY, White DJ, Hartenstein V, Eliceiri K, Tomancak P, and Cardona A. Fiji: an open-source platform for biological-image analysis. *Nat Methods* 9: 676–682, 2012.
56. Sena LA and Chandel NS. Physiological roles of mitochondrial reactive oxygen species. *Mol Cell* 48: 158–167, 2012.
57. Son SY, Ma J, Kondou Y, Yoshimura M, Yamashita E, and Tsukihara T. Structure of human monoamine oxidase A at 2.2-A resolution: the control of opening the entry for substrates/inhibitors. *Proc Natl Acad Sci U S A* 105: 5739–5744, 2008.
58. Sorato E, Menazza S, Zulian A, Sabatelli P, Gualandi F, Merlini L, Bonaldo P, Canton M, Bernardi P, and Di Lisa F. Monoamine oxidase inhibition prevents mitochondrial dysfunction and apoptosis in myoblasts from patients with collagen VI myopathies. *Free Radic Biol Med* 75: 40–47, 2014.
59. Spinazzi M, Cazzola S, Bortolozzi M, Baracca A, Loro E, Casarin A, Solaini G, Sgarbi G, Casalena G, Cenacchi G, Malena A, Frezza C, Carrara F, Angelini C, Scorrano L, Salviati L, and Vergani L. A novel deletion in the GTPase domain of OPA1 causes defects in mitochondrial morphology and distribution, but not in function. *Hum Mol Genet* 17: 3291–3302, 2008.
60. Steinberg JS, Cohen AJ, Wasserman AG, Cohen P, and Ross AM. Acute arrhythmogenicity of doxorubicin administration. *Cancer* 60: 1213–1218, 1987.
61. Steinberg SF. Oxidative stress and sarcomeric proteins. *Circ Res* 112: 393–405, 2013.
62. Sterba M, Popelova O, Vavrova A, Jirkovsky E, Kovarikova P, Gersl V, and Simunek T. Oxidative stress, redox signaling, and metal chelation in anthracycline cardiotoxicity and pharmacological cardioprotection. *Antioxid Redox Signal* 18: 899–929, 2013.
63. Sun A, Cheng Y, Zhang Y, Zhang Q, Wang S, Tian S, Zou Y, Hu K, Ren J, and Ge J. Aldehyde dehydrogenase 2 ameliorates doxorubicin-induced myocardial dysfunction through detoxification of 4-HNE and suppression of autophagy. *J Mol Cell Cardiol* 71: 92–104, 2014.
64. Tebbi CK, London WB, Friedman D, Villaluna D, De Alarcon PA, Constine LS, Mendenhall NP, Sposto R, Chauvenet A, and Schwartz CL. Dexrazoxane-associated risk for acute myeloid leukemia/myelodysplastic syndrome and other secondary malignancies in pediatric Hodgkin's disease. *J Clin Oncol* 25: 493–500, 2007.
65. Thorn CF, Oshiro C, Marsh S, Hernandez-Boussard T, McLeod H, Klein TE, and Altman RB. Doxorubicin pathways: pharmacodynamics and adverse effects. *Pharmacogenet Genomics* 21: 440–446, 2011.
66. Timolati F, Ott D, Pentassuglia L, Giraud MN, Perriard JC, Suter TM, and Zuppinger C. Neuregulin-1 beta attenuates doxorubicin-induced alterations of excitation-contraction coupling and reduces oxidative stress in adult rat cardiomyocytes. *J Mol Cell Cardiol* 41: 845–854, 2006.
67. Tonolo F, Folda A, Cesaro L, Scalcon V, Marin O, Ferro S, Bindoli A, and Rigobello MP. Milk-derived bioactive peptides exhibit antioxidant activity through the Keap1-Nrf2 signaling pathway. *J Funct Foods* 64: 2020.
68. Tonolo F, Sandre M, Ferro S, Folda A, Scalcon V, Scutari G, Feller E, Marin O, Bindoli A, and Rigobello MP. Milk-derived bioactive peptides protect against oxidative stress in a Caco-2 cell model. *Food Funct* 9: 1245–1253, 2018.
69. Wallace KB, Sardao VA, and Oliveira PJ. Mitochondrial determinants of doxorubicin-induced cardiomyopathy. *Circ Res* 126: 926–941, 2020.
70. Wang F, He Q, Sun Y, Dai X, and Yang XP. Female adult mouse cardiomyocytes are protected against oxidative stress. *Hypertension* 55: 1172–1178, 2010.
71. Wu JB, Shao C, Li X, Li Q, Hu P, Shi C, Li Y, Chen YT, Yin F, Liao CP, Stiles BL, Zhau HE, Shih JC, and Chung LW. Monoamine oxidase A mediates prostate tumorigenesis and cancer metastasis. *J Clin Invest* 124: 2891–2908, 2014.
72. Yagi K. Assay for blood plasma or serum. *Methods Enzymol* 105: 328–331, 1984.
73. Zhou S, Starkov A, Froberg MK, Leino RL, and Wallace KB. Cumulative and irreversible cardiac mitochondrial

dysfunction induced by doxorubicin. *Cancer Res* 61: 771–777, 2001.
74. Zou Y, Yao A, Zhu W, Kudoh S, Hiroi Y, Shimoyama M, Uozumi H, Kohmoto O, Takahashi T, Shibasaki F, Nagai R, Yazaki Y, and Komuro I. Isoproterenol activates extracellular signal-regulated protein kinases in cardiomyocytes through calcineurin. *Circulation* 104: 102–108, 2001.

Address correspondence to:
Prof. Fabio Di Lisa
Department of Biomedical Sciences
University of Padova
Via U.Bassi 58/B
Padova 35131
Italy

E-mail: dilisa@bio.unipd.it

Dr. Nina Kaludercic
Neuroscience Institute
National Research Council of Italy (CNR)
Via Ugo Bassi 58/B
Padova 35131
Italy

E-mail: nina.kaludercic@unipd.it

Date of first submission to ARS Central, November 4, 2019; date of final revised submission, May 25, 2020; date of acceptance, June 8, 2020.

Abbreviations Used

ΔΨm = mitochondrial membrane potential
AM = acetoxymethyl
AMVMs = adult mouse ventricular myocytes
BSA = bovine serum albumin
BW = body weight
DC = doxorubicin cardiotoxicity
DMEM = Dulbecco's modified Eagle's medium
DMSO = dimethyl sulfoxide
DTNB = 5,5′-dithiobis(2-nitrobenzoic acid)
EC = excitation-contraction
EF = ejection fraction
ETC = electron transport chain
FBS = fetal bovine serum
FCCP = carbonyl cyanide-*p*-trifluorometh oxyphenylhydrazone
FS = fractional shortening
GSSG/GSH = glutathione disulfide/glutathione
HRP = horseradish peroxidase
IVS = interventricular septum
KD = knock down
LDH = lactic dehydrogenase
LV = left ventricle
LVEDD = left ventricular end-diastolic dimension
LVESD = left ventricular end-systolic dimension
LVmass/BW = left ventricular mass normalized to body weight
LVPW = left ventricular posterior wall
MAOs = monoamine oxidases
MDA = malondialdehyde
MES = 2-(N-Morpholino) ethanesulfonic acid
MTR = MitoTracker Red
NRVMs = neonatal rat ventricular myocytes
PBS = phosphate-buffered saline
PTA = phosphotungstic acid
PTP = permeability transition pore
ROI = region of interest
ROS = reactive oxygen species
SDS = sodium dodecyl sulfate
SEM = standard error of the mean
SR = sarcoplasmic reticulum
TEM = transmission electron mycroscopy
TMRM = tetramethylrhodamine

Supplementary Data

SUPPLEMENTARY FIG. S1. Effects of MAO inhibition on mitochondrial or cytosolic oxidative status. (A) Cytosolic H_2O_2 formation measured by Cyto-HyPer in isolated NRVMs treated with 0.5 μM doxorubicin for 24 h, in the presence or absence of 100 μM pargyline. Cells have been further stimulated with increasing concentrations of H_2O_2 (i.e., 1–10–100 μM) for 10 min. $^{*}p < 0.001$ *versus* Basal by one-way ANOVA with *post hoc* Tukey's multiple comparison test. **(B)** Western blot representing the efficiency of different concentrations of MAO-A siRNA (i.e., 20–40–60 pmol) compared with scramble (Scr) in NRVMs. **(C)** GSSG/GSH ratio measured in isolated NRVMs treated with 0.5 μM doxorubicin for 24 h, in the presence or absence of 100 μM pargyline. $^{*}p < 0.05$ *versus* Untreated, $^{\#}p < 0.05$ *versus* Doxo by one-way ANOVA with *post hoc* Tukey's multiple comparison test. **(D)** Total thiol oxidation status in isolated NRVMs treated with 0.5 μM doxorubicin for 24 h, in the presence or absence of 100 μM pargyline. **(E)** AMVMs treated with 0.5 μM doxorubicin for 24 h, in the presence or absence of 200 μM pargyline. In all conditions, cells were treated with 100 μM of H_2O_2 for 10 min, and rod-shaped AMVMs have been quantified. $^{*}p < 0.001$ *versus* Untreated, $^{\#}p < 0.001$ *versus* Doxo by one-way ANOVA with *post hoc* Tukey's multiple comparison test. **(F)** Western blot representing the expression level of MAO-A in NRVMs treated with or without 0.5 μM doxorubicin for 24 h. The expression level of MAO-A has been analyzed by densitometry analysis and normalized to actin. **(G)** Western blot representing the expression level of MAO-B in AMVMs treated with or without 0.5 μM doxorubicin for 24 h. The expression level of MAO-A has been analyzed by densitometry analysis and normalized to actin. **(H)** Mitochondrial H_2O_2 formation measured by Mito-HyPer in isolated NRVMs treated with 0.5 μM doxorubicin for 24 h, in the presence or absence of 100 μM pargyline. Cells have been further stimulated with 20 μM tyramine for 2 h. $^{*}p < 0.05$ *versus* Untreated Vehicle, $^{\#}p < 0.001$ *versus* Untreated Tyramine, $^{\S}p < 0.001$ *versus* Doxo Tyramine, $^{\$}p < 0.001$ *versus* Vehicle by one-way ANOVA with *post hoc* Tukey's multiple comparison test. Approximately 30 cells were analyzed per condition in each experiment, and all the experiments were performed at least three times using three different animal or cell preparations. The GSSG/GSH ratio measurement, the total thiol estimation, and Western blot analyses were performed three times using three different animal preparations. Data are expressed as mean ± SEM. Integral blots are shown in Supplementary Figure S2. MAO, monoamine oxidase; NRVM, neonatal rat ventricular myocyte; SEM, standard error of the mean.

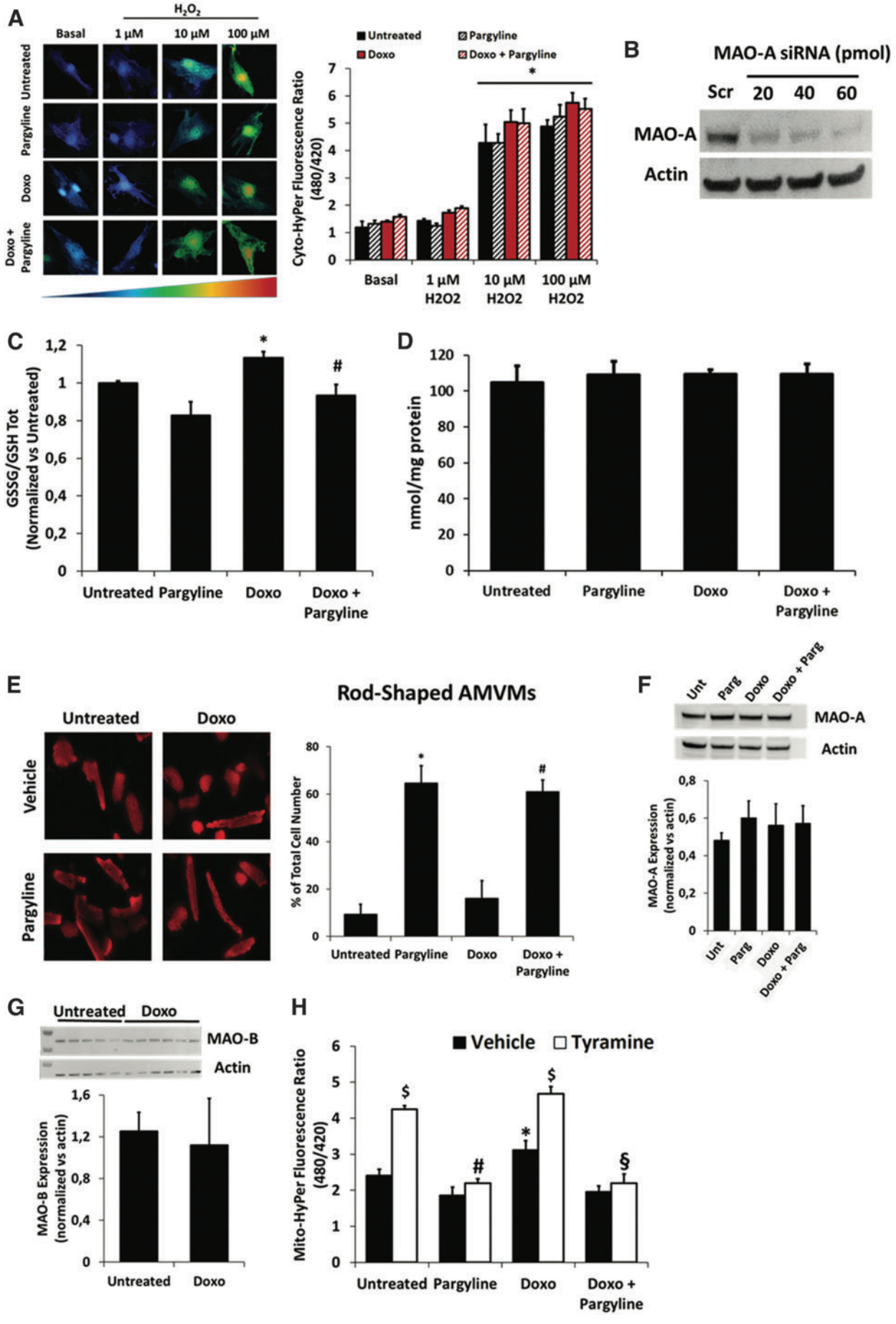
A
H_2O_2
Basal
1 µM
10 µM
100 µM
Untreated
Pargyline
Doxo
Doxo + Pargyline
Cyto-HyPer Fluorescence Ratio (480/420)
Basal
1 µM H2O2
10 µM H2O2
100 µM H2O2
B
MAO-A siRNA (pmol)
Scr
20
40
60
MAO-A
Actin
C
GSSG/GSH Tot (Normalized vs Untreated)
Untreated
Pargyline
Doxo
Doxo + Pargyline
D
nmol/mg protein
Untreated
Pargyline
Doxo
Doxo + Pargyline
E
Untreated
Doxo
Vehicle
Pargyline
Rod-Shaped AMVMs
% of Total Cell Number
Untreated
Pargyline
Doxo
Doxo + Pargyline
F
Unt
Parg
Doxo
Doxo + Parg
MAO-A
Actin
MAO-A Expression (normalized vs actin)
G
Untreated
Doxo
MAO-B
Actin
MAO-B Expression (normalized vs actin)
H
Vehicle
Tyramine
Mito-HyPer Fluorescence Ratio (480/420)
Untreated
Pargyline
Doxo
Doxo + Pargyline

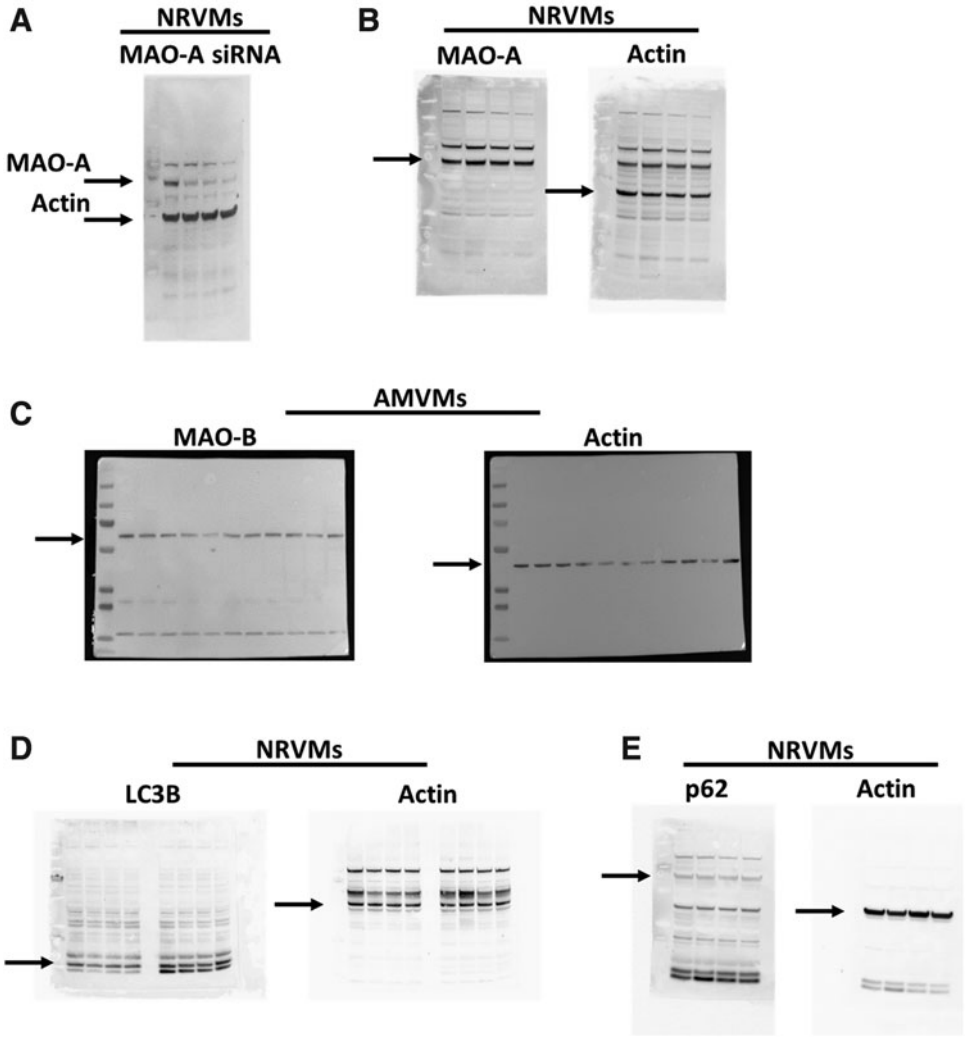

SUPPLEMENTARY FIG. S2. Original images of cropped Western blots. **(A)** Western blot representing the efficiency of different concentrations of MAO-A siRNA (i.e., 20–40–60 pmol) compared with scramble (Scr) in NRVMs. The image refers to Supplementary Figure S1B. **(B)** Western blot representing the expression level of MAO-A in NRVMs treated with or without 0.5 μM doxorubicin for 24 h. The image refers to Supplementary Figure S1F. **(C)** Western blot representing the expression level of MAO-B in AMVMs treated with or without 0.5 μM doxorubicin for 24 h. The image refers to Supplementary Figure S1G. **(D)** Western blot representing LC3B-II abundance in isolated NRVMs treated with 0.5 μM doxorubicin for 24 h, in the presence or absence of 100 μM pargyline. The image refers to Supplementary Figure S3D. **(E)** Western blot representing p62 expression levels in isolated NRVMs treated with 0.5 μM doxorubicin for 24 h, in the presence or absence of 100 μM pargyline. The image refers to Supplementary Figure S3E.

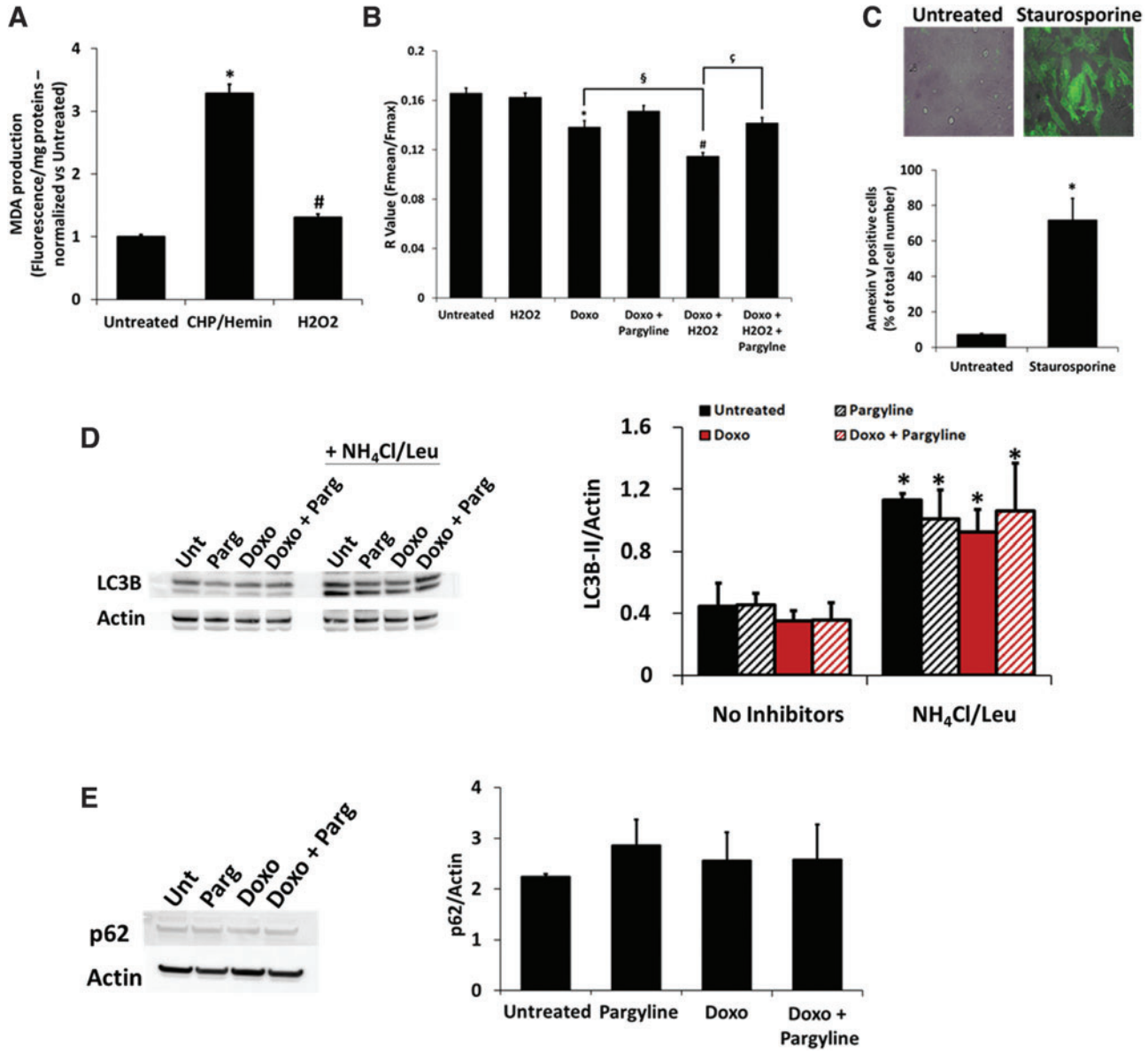

SUPPLEMENTARY FIG. S3. Effects of MAO inhibition on mitochondrial and cell function and morphology. (A) MDA formation in isolated NRVMs treated with 25 m*M* CHP and 50 μM hemin for 15 min, or with 100 μM H_2O_2 for 1 h. Raw fluorescence values were normalized to milligram proteins, and then normalized *versus* Untreated. $^{*}p < 0.001$ *versus* Untreated, $^{\#}p < 0.05$ *versus* Untreated by one-way ANOVA with *post hoc* Tukey's multiple comparison test. **(B)** Average of mitochondrial distribution representing *R* value evaluated in isolated NRVMs treated with 0.5 μM doxorubicin for 24 h, in the presence or absence of 100 μM pargyline. Cells have been further stimulated with 10 μM H_2O_2 for 1 h. $^{*}p < 0.01$, $^{\#}p < 0.001$ *versus* Untreated, $^{\S}p < 0.01$ *versus* Doxo, $^{\varsigma}p < 0.01$ *versus* Doxo+H_2O_2 by one-way ANOVA with *post hoc* Tukey's multiple comparison test. Where data were not normally distributed, the Kruskal–Wallis test has been applied. **(C)** Apoptosis evaluated by Annexin-V-Fluos staining in isolated NRVMs treated with 2 μM staurosporine for 1 h. Histogram displays the percentage of Annexin V-positive cells normalized to the total number of cells identified by bright-field images. $^{*}p < 0.001$ *versus* Untreated by the Kruskal–Wallis test. **(D)** LC3B-II abundance in isolated NRVMs treated with 0.5 μM doxorubicin for 24 h, in the presence or absence of 100 μM pargyline. Cells have been also incubated with inhibitors of lysosomal degradation for 4 h (i.e., 20 m*M* NH_4Cl, 100 μM Leupeptin). $^{*}p < 0.05$ *versus* No inhibitors by one-way ANOVA with *post hoc* Tukey's multiple comparison test. **(E)** p62 expression levels in isolated NRVMs treated with 0.5 μM doxorubicin for 24 h, in the presence or absence of 100 μM pargyline. For the evaluation of the *R* parameter, $\sim$30 cells were analyzed per condition in each experiment. For the evaluation of apoptosis, $\sim$100 cells were analyzed per condition in each experiment. All the experiments were performed three times using three different animal preparations. Western blot analyses were performed six times using six different animal preparations. Data are expressed as mean $\pm$ SEM. Integral blots are shown in Supplementary Figure S2. CHP, cumene hydroperoxide; MDA, malondialdehyde.